




Reducing oxidative protein folding alleviates senescence by minimizing ER-to-nucleus H₂O₂ release

Fang Cheng^{1,2,†} , Qianzhao Ji^{2,3,†}, Lu Wang¹, Chih-chen Wang^{1,2}, Guang-Hui Liu^{2,3,4,5,*}  & Lei Wang^{1,2,**} 

Abstract

Oxidative protein folding occurs in the endoplasmic reticulum (ER) to generate disulfide bonds, and the by-product is hydrogen peroxide (H₂O₂). However, the relationship between oxidative protein folding and senescence remains uncharacterized. Here, we find that the protein disulfide isomerase (PDI), a key oxidoreductase that catalyzes oxidative protein folding, accumulated in aged human mesenchymal stem cells (hMSCs) and deletion of PDI alleviated hMSCs senescence. Mechanistically, knocking out *PDI* slows the rate of oxidative protein folding and decreases the leakage of ER-derived H₂O₂ into the nucleus, thereby decreasing the expression of *SERPINE1*, which was identified as a key driver of cell senescence. Furthermore, we show that depletion of PDI alleviated senescence in various cell models of aging. Our findings reveal a previously unrecognized role of oxidative protein folding in promoting cell aging, providing a potential target for aging and aging-related disease intervention.

Keywords human mesenchymal stem cells (hMSCs); hydrogen peroxide (H₂O₂); oxidative protein folding; protein disulfide isomerase (PDI); senescence

Subject Categories Molecular Biology of Disease; Translation & Protein Quality

DOI 10.15252/embr.202256439 | Received 7 November 2022 | Revised 18 May 2023 | Accepted 26 May 2023 | Published online 12 June 2023

EMBO Reports (2023) 24: e56439

Introduction

Stem cell exhaustion is considered one of the hallmarks of aging (Cai *et al.*, 2022; Lopez-Otin *et al.*, 2023). Mesenchymal stem cells (MSCs) are adult stem cells that show self-renewal capacity and can

differentiate into different mesodermal lineages, such as chondrocytes, osteoblasts, and adipocytes (Ullah *et al.*, 2015). Therefore, MSCs have been extensively applied to tissue engineering and regenerative medicine (Li *et al.*, 2017; Han *et al.*, 2019; Wang *et al.*, 2022a). However, the functions of MSCs progressively decline during aging, a process involving lost maintenance of tissue homeostasis, which induces aging-associated tissue degeneration. (Li *et al.*, 2017; Deng *et al.*, 2019; Fraile *et al.*, 2022; Sun *et al.*, 2022b). Therefore, understanding the molecular processes involved in MSCs senescence is crucial to identify novel therapeutic targets for the treatment of aging-related degeneration.

Proteostasis enables healthy cell and organismal development and protects against disease (Balch *et al.*, 2008). Impaired protein homeostasis is linked to aging and aging-related diseases (Hipp *et al.*, 2019). Studies have revealed that reducing protein synthesis (Tavernarakis, 2008; Papadopoli *et al.*, 2019) and boosting the protein quality control system (Higuchi-Sanabria *et al.*, 2018; Ghosh *et al.*, 2020; Zhang *et al.*, 2022b) can ameliorate aging-related diseases and extend the life span. However, little is known about the relationship between the protein folding rate and aging. A unique process of protein folding is oxidative protein folding, which is critical for the formation of disulfide bonds during the folding of nascent peptides into form native proteins. In eukaryotes, approximately one-third of proteins are secretory or membrane proteins, which usually form disulfide bonds and fold in the endoplasmic reticulum (ER; Wang & Wang, 2023). Oxidative protein folding is mainly catalyzed by protein disulfide isomerase (PDI) family members, which play central roles in disulfide bond oxidation, reduction, and isomerization (Bulleid & Ellgaard, 2011; Wang & Wang, 2023). Protein disulfide isomerase introduces disulfides into substrate proteins by transferring electrons to an upstream oxidase, ER oxidoreductin 1 (Ero1). Ero1 is a sulfhydryl oxidase, which uses molecular oxygen as an electron acceptor and produces disulfide with an equimolar

1 National Laboratory of Biomacromolecules, CAS Center for Excellence in Biomacromolecules, Institute of Biophysics, Chinese Academy of Sciences, Beijing, China

2 College of Life Sciences, University of Chinese Academy of Sciences, Beijing, China

3 State Key Laboratory of Membrane Biology, Institute of Zoology, Chinese Academy of Sciences, Beijing, China

4 Beijing Institute for Stem Cell and Regenerative Medicine, Beijing, China

5 Advanced Innovation Center for Human Brain Protection, National Clinical Research Center for Geriatric Disorders, Xuanwu Hospital, Capital Medical University, Beijing, China

*Corresponding author. Tel: +86 10 64807852; E-mail: ghliu@ioz.ac.cn

**Corresponding author. Tel: +86 10 64888501; E-mail: wanglei@ibp.ac.cn

[†]These authors contributed equally to this work

concentration of H₂O₂ (Bulleid & Ellgaard, 2011). It has been proposed that oxidative protein folding contributes approximately 25% of cellular reactive oxygen species (ROS) during protein synthesis (Tu & Weissman, 2004).

The excessive accumulation of ROS levels and decreased antioxidant systems can induce severe oxidative damage in lipids, DNA, and proteins, which promotes stem cell dysfunction with aging (Oh et al, 2014; Cai et al, 2022; Wang et al, 2022b). While previous studies of oxidative stress on cell senescence have mostly focused on mitochondria-derived ROS (Li et al, 2013; Vasileiou et al, 2019; Kong et al, 2022), ROS generated in the ER have been neglected for a long time. In fact, little is known about the role of oxidative protein folding in cell senescence. Since *PDI*-knockout mice are embryonic lethal (Xu et al, 2014; Parakh & Atkin, 2015), research into the role of *PDI* in aging has been hindered.

In this study, we first observed that *PDI* was accumulated in aged hMSCs. We generated *PDI*-knockout (*PDI*^{-/-}) human embryonic stem cells (hESCs) and hMSCs, and found that *PDI* deficiency attenuated cell senescence in hMSCs. By using the ultrasensitive, genetically encoded H₂O₂ sensor HyPer7, we showed that *PDI*-mediated oxidative protein folding triggered the release of H₂O₂ from the ER to the nucleus. *PDI*-H₂O₂ axis induced the accumulation of SERPINE1, which induced cell senescence. Importantly, depletion of *PDI* alleviated senescence in various cell aging models, indicating that targeting oxidative protein folding is a promising strategy for aging and aging-related disease intervention.

Results

PDI is upregulated in senescent hMSCs

To establish a link between cell senescence and *PDI*, we first detected the expression of *PDI*, the key enzyme catalyzing oxidative protein folding in the ER, in replicative senescent (RS) hMSCs, and Werner Syndrome (WS) hMSCs, which undergo premature senescence (Zhang et al, 2015). The results showed that *PDI* expression was upregulated in RS hMSCs and WS hMSCs (Fig 1A and B). In addition, *PDI* expression was also upregulated in the livers of aged mice (Fig 1C). Moreover, *PDI* was identified to be significantly upregulated with aging according to the published “senescence associated secretory phenotype (SASP) Atlas” (Basisty et al, 2020), and database of human plasma (Ritchie et al, 2021), while other members of the *PDI* family were not (Fig EV1A). These results suggest that *PDI* may be involved in cell senescence.

PDI-deficient hESCs maintain pluripotency

To study the roles of *PDI* in human stem cell aging and homeostasis, we generated *PDI*-deficient hESCs via CRISPR/Cas9-mediated gene editing technology. We obtained *PDI*-knockout (*PDI*^{-/-}) hESCs, which harbored frameshift mutations resulting in premature stop codons (Fig EV1B). The successful ablation of *PDI* protein was validated by western blotting and immunofluorescence staining (Fig 1D and E). No off-target cleavage was detected in the seven sites predicted to be most likely affected (Fig EV1C). *PDI*^{-/-} hESCs expressed pluripotency markers, including OCT4, NANOG, and SOX2 (Fig 1F). In addition, *PDI*^{-/-} hESCs maintained *in vivo* differentiation

potential toward three germ layer lineages (endoderm, mesoderm, and ectoderm), as shown by a teratoma assay (Fig EV1D). In addition, no remarkable difference in cell proliferation ability or cell cycle kinetics was detected between *PDI*^{-/-} and *PDI*^{+/+} hESCs (Figs 1G and EV1E). Moreover, a genome-wide copy number variation (CNV) analysis and karyotype analysis showed that *PDI*^{-/-} hESCs maintained genomic stability and integrity (Figs 1H and EV1F). Taken together, these results indicate that the *PDI*^{-/-} hESCs maintain normal self-renewal capability and pluripotency.

PDI deficiency alleviates hMSCs senescence

To investigate the role of *PDI* in human adult stem cells, we differentiated *PDI*^{+/+} and *PDI*^{-/-} hESCs into hMSCs, adult stem cells susceptible to senescence (Fig 2A). The *PDI*^{+/+} and *PDI*^{-/-} hMSCs expressed typical hMSC markers, such as CD73, CD90, and CD105 (Fig EV2A), but not hMSC-irrelevant markers, such as CD34, CD43, or CD45 (Fig EV2B). The differentiated hMSCs maintained genomic integrity, as revealed by a CNV analysis (Fig EV2C). Western blotting and immunofluorescence staining confirmed the loss of *PDI* protein in the *PDI*^{-/-} hMSCs (Fig 2B and C). Since *PDI* is a structural subunit of collagen prolyl 4-hydroxylases (P4H; Koivu et al, 1987; Hatahet & Ruddock, 2009), the results showing that the catalytic subunits of P4H (P4HA1 and P4HA2) were reduced in *PDI*^{-/-} hMSCs validated the loss of *PDI* (Fig EV2D). However, we did not observe a significant change in the protein levels of other *PDI* family members, such as P5, ERp46, ERp72, ERp57, or ERp44, in the *PDI*^{-/-} hMSCs (Fig 2D). The redundancy of *PDI* family proteins may account the proper oxidative protein folding and acquisition of *PDI*-deficient hMSCs.

Next, we compared the multipotent differentiation potential of *PDI*^{+/+} and *PDI*^{-/-} hMSCs and observed that the *PDI*^{-/-} hMSCs exhibited enhanced differentiation ability toward adipocytes, osteoblasts and chondrocytes compared with that of the *PDI*^{+/+} hMSCs (Fig EV2E–G). Notably, we observed that *PDI* deficiency markedly increased the cumulative population-doubling level of hMSCs during serial passaging. The growth arrest of the *PDI*^{+/+} hMSCs was evident in passage 10, but the *PDI*^{-/-} hMSCs continued to grow until passage 12 (Fig 2E). Cell clonal expansion formation and Ki67 immunostaining confirmed the increased proliferation of the *PDI*^{-/-} hMSCs (Fig 2F and G). Additionally, decreased senescence-associated β-gal (SA-β-gal) activity was detected in the *PDI*^{-/-} hMSCs (Fig 2H). We also detected reduced secretion of interleukin-6 (IL-6; Fig 2I and J), upregulated expression of nuclear lamina proteins such as LAP2 and Lamin B1 (Figs 2J and EV2H), downregulated expression of the senescence-associated marker P16 (Fig 2J and K), and increased telomere lengths (Fig 2L) in the *PDI*^{-/-} hMSCs. In addition, the DNA damage response in the *PDI*^{-/-} hMSCs was attenuated, as evidenced by a decreased percentage of 53BP1 and γH2AX double-positive cells (Fig 2M). The tibialis anterior muscle of mice has a microenvironment suitable for the survival of mesoderm cells, and there is an accelerated attrition of senescent MSCs *in vivo* (Pan et al, 2016; Deng et al, 2019). Thus, we injected *PDI*^{+/+} and *PDI*^{-/-} hMSCs transduced with a lentiviral vector expressing luciferase into the tibialis anterior muscles of immune-deficient mice and observed that, compared with *PDI*^{+/+} hMSCs, *PDI*^{-/-} hMSCs showed delayed *in vivo* attrition (Fig 2N). Reintroduction of *PDI* into *PDI*^{-/-} hMSCs (Fig EV2I) restored senescent phenotypes in

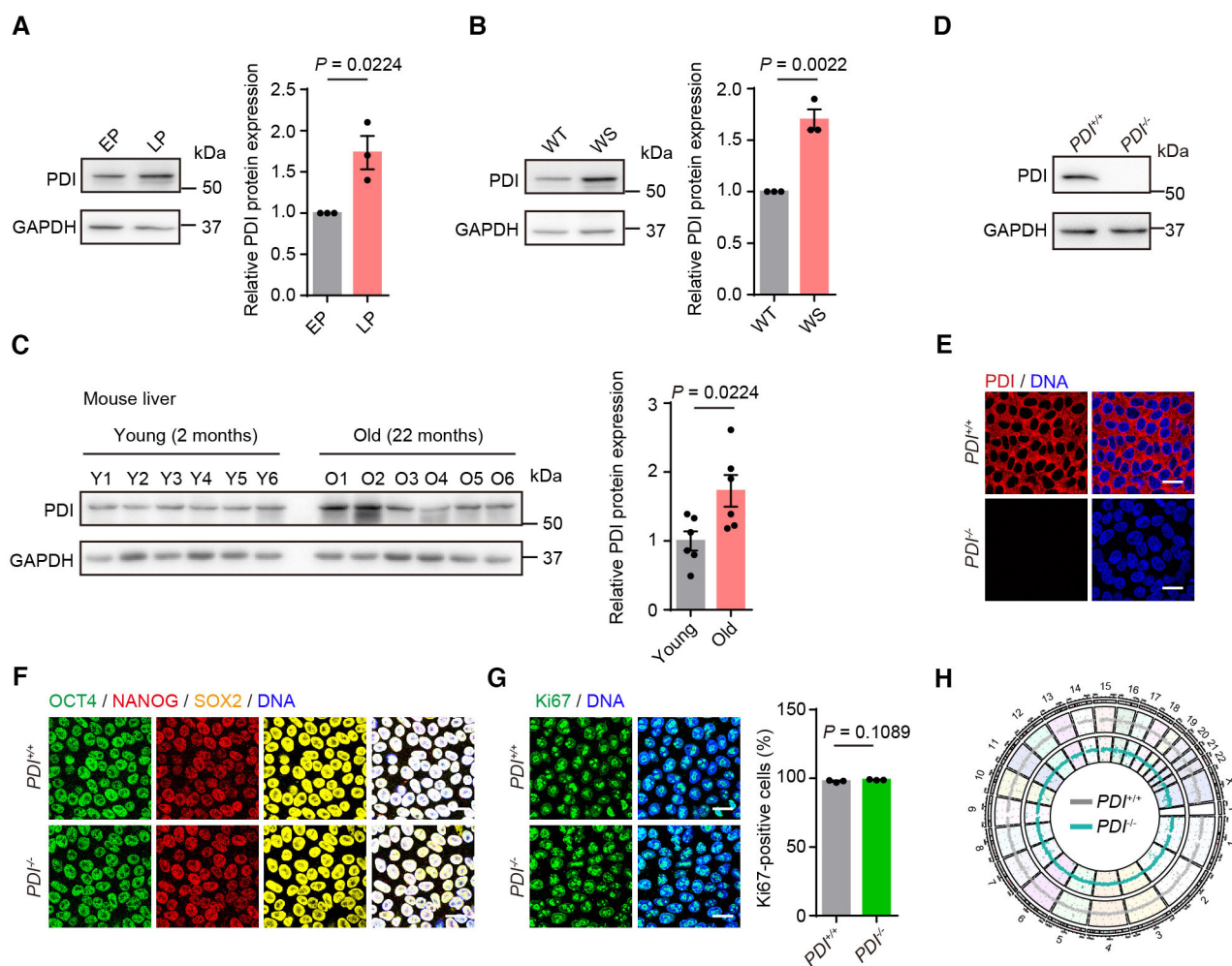


Figure 1. Generation and characterization of $PDI^{-/-}$ hESCs.

- A Left, western blotting of PDI protein in replicative senescent hMSCs at early-passage (EP) and late-passage (LP). GAPDH was used as the loading control. Right, statistical analysis of relative PDI protein expression levels. $n = 3$ independent experiments.
- B Left, western blotting of PDI protein in wild-type (WT) and Werner syndrome (WS) hMSCs. GAPDH was used as the loading control. Right, statistical analysis of relative PDI protein expression levels. $n = 3$ independent experiments.
- C Left, western blotting of PDI protein in the liver of mice at young (2 months) and old (22 months) ages. GAPDH was used as the loading control. Right, statistical analysis of relative PDI protein expression levels. $n = 6$ mice.
- D Western blotting of PDI expression in $PDI^{+/+}$ and $PDI^{-/-}$ hESCs. GAPDH was used as the loading control.
- E Immunostaining of PDI in $PDI^{+/+}$ and $PDI^{-/-}$ hESCs. Scale bar, 25 μm .
- F Immunostaining of OCT4, NANOG and SOX2 in $PDI^{+/+}$ and $PDI^{-/-}$ hESCs. Scale bar, 25 μm .
- G Left, Ki67 staining of $PDI^{+/+}$ and $PDI^{-/-}$ hESCs. Scale bar, 25 μm . Right, statistical analysis of Ki67-positive cells. $n = 3$ independent experiments.
- H Genome wide analysis of copy number variations (CNVs) of $PDI^{+/+}$ and $PDI^{-/-}$ hESCs.

Data information: In (A–C, G), data are presented as mean \pm SEM, two-tailed Student's t -test. Source data are available online for this figure.

stem cells, as indicated by a decrease in clonal formation ability and the number of Ki67-positive cells, as well as an increase in the number of SA- β -gal-positive cells (Fig 20–Q).

PDI deficiency slows the rate of oxidative protein folding and reduces the level of its byproduct, H_2O_2

Since PDI is a key oxidoreductase, we aimed to determine the effect of PDI on cellular redox homeostasis. ER-, cytosol- and

mitochondrion-localized redox-sensitive green fluorescent proteins (roGFPs) were used to monitor subcellular glutathione redox conditions in live cells. The ratio of fluorescence intensity at 390/465 nm (for roGFP-ER) or 405/488 nm (for roGFP-cytosol and roGFP-mitochondria) excitation increases under oxidizing conditions and decreases under reducing conditions (Wu *et al.*, 2019). The results showed that deletion of PDI slightly reduced the ER but exerted no effect on the glutathione redox state of the cytosol or mitochondria (Fig EV3A–C), probably due to the functional redundancy of PDI

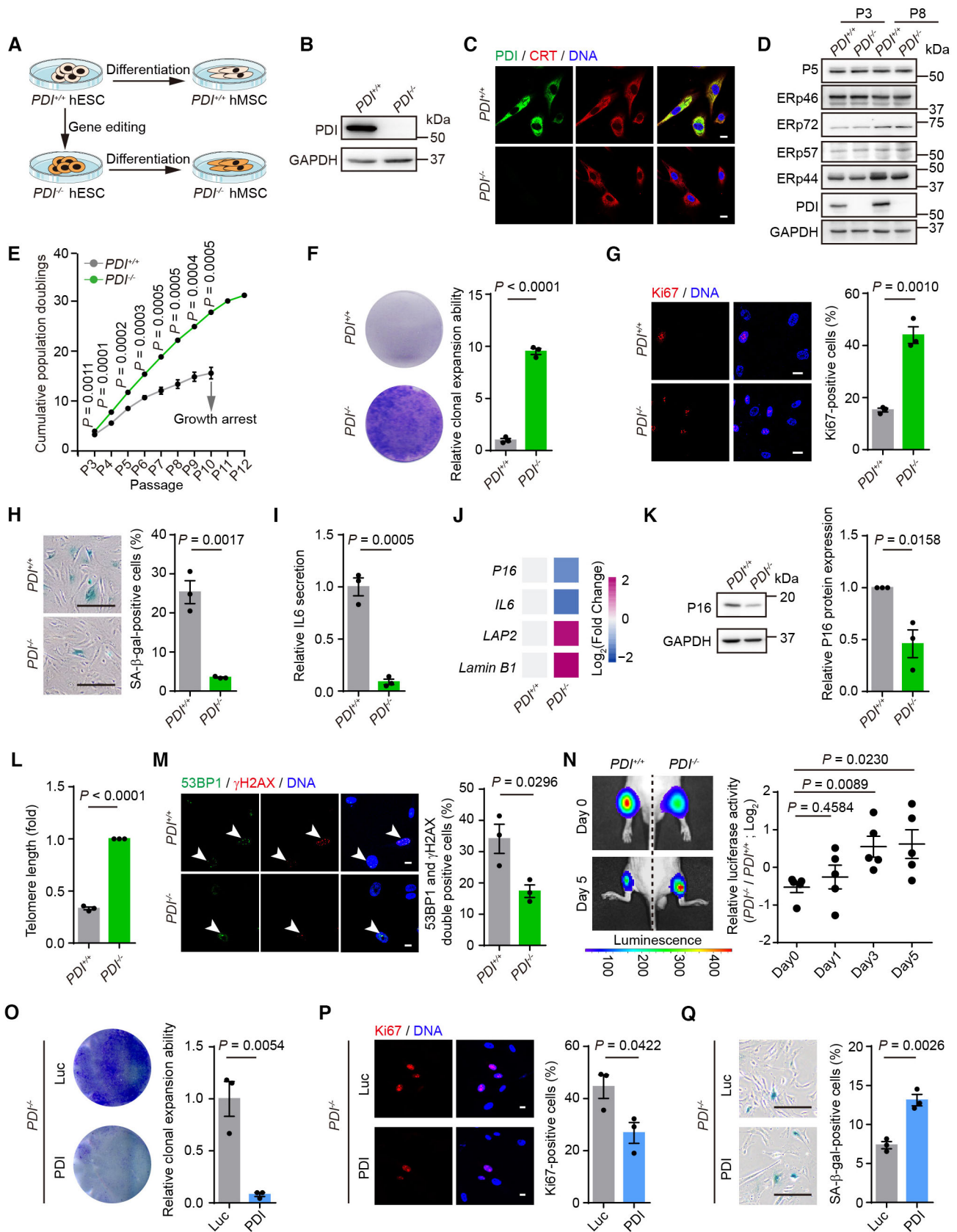


Figure 2.

Figure 2. PDI deficiency alleviates hMSCs senescence.

- A Schematic representation of differentiation $PDI^{+/+}$ and $PDI^{-/-}$ hESCs into hMSCs.
- B Western blotting of PDI protein in $PDI^{+/+}$ and $PDI^{-/-}$ hMSCs. GAPDH was used as the loading control.
- C Immunostaining of PDI and calreticulin (CRT) in $PDI^{+/+}$ and $PDI^{-/-}$ hMSCs, CRT was used as ER marker. Scale bar, 25 μ m.
- D Western blotting analysis of PDI family members expression in $PDI^{+/+}$ and $PDI^{-/-}$ hMSCs at early-passage (P3) and late-passage (P8). GAPDH was used as the loading control.
- E Growth curve showing the cumulative population doublings of $PDI^{+/+}$ and $PDI^{-/-}$ hMSCs. $n = 3$ biological repeats.
- F Single clonal formation of $PDI^{+/+}$ and $PDI^{-/-}$ hMSCs at P8. $n = 3$ biological repeats.
- G Left, Ki67 staining of $PDI^{+/+}$ and $PDI^{-/-}$ hMSCs at P8. Scale bar, 20 μ m. Right, statistical analysis of Ki67-positive cells. $n = 3$ biological repeats.
- H Left, SA- β -gal staining of $PDI^{+/+}$ and $PDI^{-/-}$ hMSCs at P8. Scale bar, 200 μ m. Right, statistical analysis of SA- β -gal-positive cells. $n = 3$ biological repeats.
- I ELISA analysis for IL6 secretion in $PDI^{+/+}$ and $PDI^{-/-}$ hMSCs at P8. $n = 3$ biological repeats.
- J Heatmap showing the mRNA levels of *P16*, *IL6*, *LAP2* and *Lamin B1* in $PDI^{+/+}$ and $PDI^{-/-}$ hMSCs at P8. Colors from blue to red represent the levels of gene expression from low to high. $n = 3$ independent repeats.
- K Left, western blotting showing the P16 expression in $PDI^{+/+}$ and $PDI^{-/-}$ hMSCs at P8. GAPDH was used as the loading control. Right, statistical analysis of relative P16 protein expression levels. $n = 3$ independent experiments.
- L qPCR analysis of the telomere length of $PDI^{+/+}$ and $PDI^{-/-}$ hMSCs at P8. $n = 3$ independent experiments.
- M Left, Immunostaining of 53BP1 and γ H2AX in $PDI^{+/+}$ and $PDI^{-/-}$ hMSCs at P8. White arrowheads indicate 53BP1 and γ H2AX double-positive cells. Right, statistical analysis of 53BP1 and γ H2AX double-positive cells. Scale bar, 10 μ m. $n = 3$ biological repeats.
- N Luciferase activity analysis in the tibialis anterior muscles of nude mice transplanted with $PDI^{+/+}$ or $PDI^{-/-}$ hMSCs that expressed luciferase. Luciferase activity was detected at days 0, 1, 3, 5. Left, representative images showing the luciferase activity at day 0 and 5. Right, statistical analysis of the luciferase activity in each day. $n = 5$ mice.
- O Single clonal formation analysis of the $PDI^{-/-}$ hMSCs transduced with lentiviruses expressing luciferase (Luc) or PDI. $n = 3$ biological repeats.
- P Left, Ki67 staining of $PDI^{-/-}$ hMSCs transduced with lentiviruses expressing Luc or PDI. Scale bar, 10 μ m. Right, statistical analysis of Ki67-positive cells. $n = 3$ biological repeats.
- Q Left, SA- β -gal staining of $PDI^{-/-}$ hMSCs transduced with lentiviruses expressing Luc or PDI. Scale bar, 200 μ m. Right, statistical analysis of SA- β -gal-positive cells. $n = 3$ biological repeats.

Data information: In (E–I, K–Q), data are presented as mean \pm SEM, two-tailed Student's *t*-test. Source data are available online for this figure.

family proteins involved the maintenance of redox homeostasis. As Ero1 α -PDI constitutes the pivotal oxidative folding pathway in the ER (Bulleid & Ellgaard, 2011; Zhang et al, 2014), we wondered whether PDI deficiency affects the efficacy of oxidative protein folding. Similar to that of PDI, the expression of Ero1 α was increased in RS hMSCs and was suppressed by PDI deletion (Fig EV3D). Furthermore, we used a dithiothreitol (DTT) pulse-chase assay to monitor the oxidative folding process of the immunoglobulin J-chain, which forms three intrachain disulfide bonds (Zhang et al, 2018). PDI deficiency slowed the rate at which the reduced J-chain disappeared, and fewer oxidized dimers or high-molecular-weight species accumulated (Fig 3A and B). Similar to the folding of J-chain, loss of PDI also slowed the oxidative folding rate of low-density lipoprotein receptor (LDLR), a cysteine-rich protein (Kadokura et al, 2020; Fig EV3E).

The by-product of Ero1 α -PDI-mediated oxidative protein folding is H₂O₂ (Fig 3C). Since the accumulation of excess H₂O₂ has been reported to cause oxidative stress and induce hMSCs senescence (Burova et al, 2013), we reasoned that the slow oxidative protein folding in the absence of PDI helps to attenuate the excessive accumulation of H₂O₂ and thus delay cell senescence. Therefore, the ER-localized H₂O₂ probe HyPer-ER was used to measure the levels of H₂O₂ in the ER. The fluorescence intensity ratio at 488/405 nm excitation largely decreased in $PDI^{-/-}$ hMSCs, indicating relatively a low oxidation rate of the HyPer-ER probe (Fig 3D). Because the HyPer-ER probe can be oxidized by either H₂O₂ or by disulfides in the ER (Ramming et al, 2014), a low dose of DTT (0.5 mM) was added to exclude the oxidative effect exerted by disulfides (Zhang et al, 2019b). Then, we observed that the levels of H₂O₂ in the ER lumen of the $PDI^{-/-}$ hMSCs were much lower than those in the $PDI^{+/+}$ cells (Fig 3D). An Amplex Red assay confirmed the decreased overall H₂O₂ levels in the lysates of $PDI^{-/-}$ hMSCs (Fig 3E).

Moreover, the total ROS levels were reduced in the $PDI^{-/-}$ hMSCs, as determined by H₂DCFDA staining (Fig 3F).

To validate the finding showing that the decrease in H₂O₂ levels in the $PDI^{-/-}$ hMSCs was mediated by PDI, we reconstituted the oxidative protein folding system *in vitro* with purified proteins. In addition to PDI, four other constitutively expressed PDI family members, P5, ERp46, ERp72, and ERp57, each of which harbors at least two -CGHC- active sites critical for catalyzing the thiol-disulfide interchange reaction (Wang et al, 2021), were analyzed (Fig 3G). An oxygen electrode was used to monitor the oxygen consumption during the oxidation of the PDIs mediated by Ero1 α in the presence of GSH, the electron donor. Ero1 α oxidized the other PDIs slowly, and the addition of PDI markedly increased the oxygen consumption rate (Fig 3H). Moreover, the presence of PDI increased the production of H₂O₂, as monitored by Amplex Red assay (Fig 3I). Altogether, our data indicate that PDI deficiency slows the rate of oxidative protein folding and reduces the rate of H₂O₂ production in the ER.

The ER-to-nucleus release of H₂O₂ is attenuated by PDI deletion

Whether ER-derived H₂O₂ is released and affects surrounding organelles, including the nucleus to regulate the gene expression profile during aging, remained unclear. As H₂O₂ can be rapidly eliminated by peroxidases and peroxiredoxins in the cytosol and nucleus, we employed a recently developed ultrasensitive H₂O₂ sensor, HyPer7 (Pak et al, 2020; Hoehne et al, 2022), to detect the diffusion of ER-derived H₂O₂. HyPer7 was targeted to the nucleus or cytosol (Fig EV3F), and the fluorescence intensity ratio at 500/400 nm excitation was monitored (Figs 3J and EV3G). DTT treatment mimics the burst of free thiols during protein synthesis and profoundly activates H₂O₂ generation by the Ero1 α -PDI oxidative protein folding

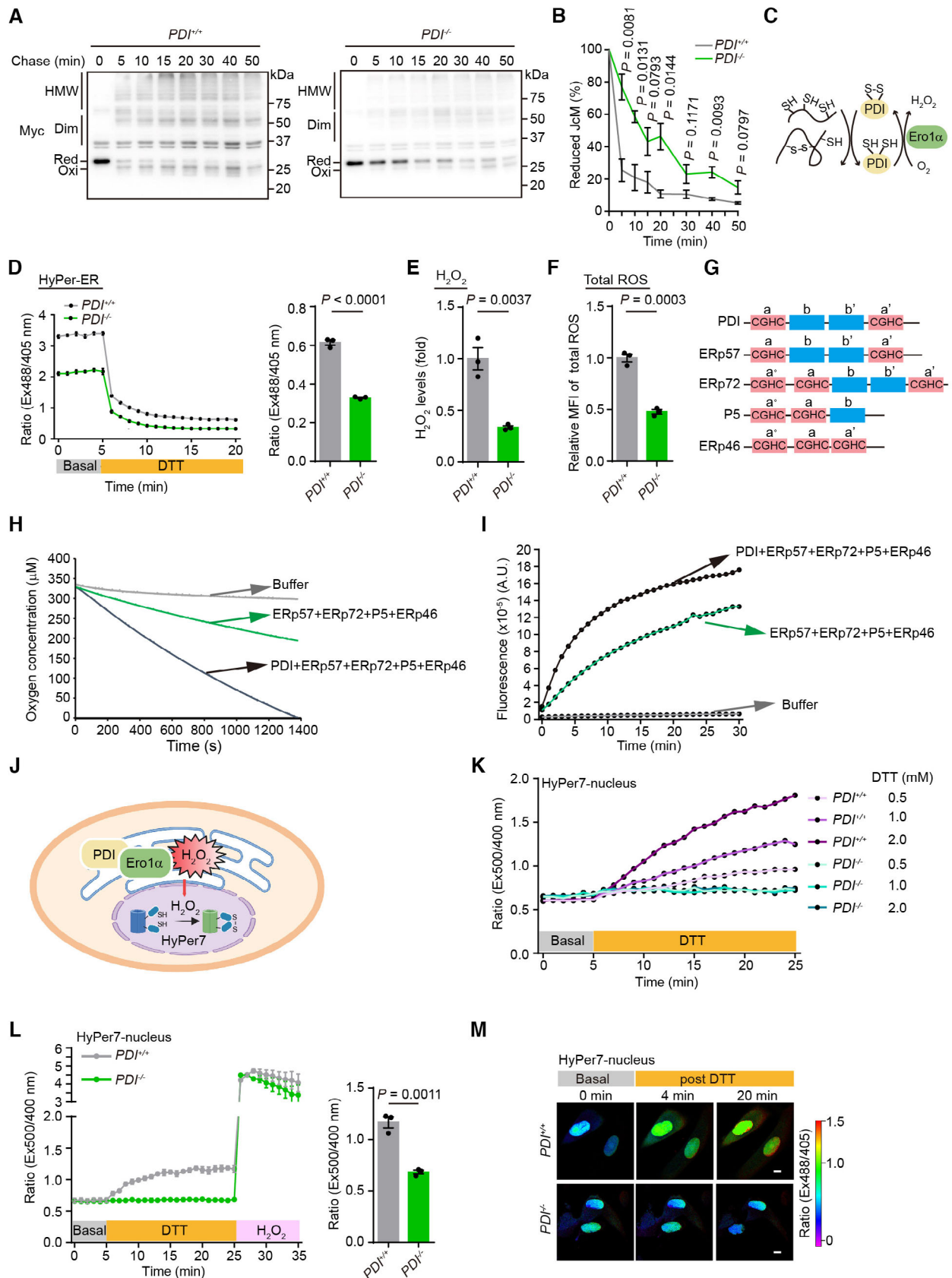


Figure 3.

Figure 3. Deficiency of PDI slows the rate of oxidative protein folding and reduces its byproduct H₂O₂.

- A Oxidative folding of Myc-tagged J-Chain (JcM). *PDI*^{+/+} and *PDI*^{-/-} hMSCs were transfected with JcM for 48 h, then were pulsed with DTT and chased at indicated time after DTT removal. The lysates were analyzed using non-reducing SDS-15% PAGE and α -Myc western blotting. The mobilities of reduced JcM monomers (Red), oxidized monomers (Oxi), homodimers (Dim), and high-molecular-weight (HMW) species are indicated.
- B The fraction of reduced JcM (Red/[Red + Oxi]) in (A) was quantified by densitometry. *n* = 3 independent experiments.
- C Model of the Ero1 α -PDI oxidative protein folding pathway.
- D Time-dependent changes of H₂O₂ levels in the ER of *PDI*^{+/+} and *PDI*^{-/-} hMSCs at P8. Left, the fluorescence intensity ratio of HyPer-ER at 535 nm with excitation at 488 and 405 nm was first monitored at resting state for 5 min, followed by addition of 0.5 mM DTT (yellow bar) for another 15 min. Right, statistical analysis of the fluorescence intensity ratio at 488/405 nm excitation of HyPer-ER probe at 15 min post DTT addition. *n* = 3 independent experiments.
- E Analysis of the H₂O₂ levels in *PDI*^{+/+} and *PDI*^{-/-} hMSCs at P8 using Amplex Red assays. *n* = 3 biological repeats.
- F Analysis of the cellular total ROS levels in *PDI*^{+/+} and *PDI*^{-/-} hMSCs at P8 using H₂DCFDA probe. *n* = 3 biological repeats.
- G Schematic representation of the PDI family members. The -CGHC- active sites in the catalytic domains are indicated.
- H Oxygen consumption by 1 μ M purified Ero1 α protein was monitored by using an oxygen electrode in the presence of PDI proteins (each 10 μ M) and 10 mM GSH.
- I H₂O₂ produced by Ero1 α -PDIs system were detected using Amplex Red assays.
- J Schematic diagram showing the detection of the nuclear H₂O₂ by HyPer7-nucleus upon activation of the Ero1 α -PDI oxidative protein folding system in the ER.
- K Response of HyPer7-nucleus probes in *PDI*^{+/+} and *PDI*^{-/-} hMSCs. The fluorescence intensity ratio of HyPer7-nucleus at 520 nm with excitation at 500/400 nm was firstly monitored at resting state for 5 min, followed by addition of different concentrations of DTT (yellow bar) for another 20 min.
- L Left, response of HyPer7-nucleus probes in *PDI*^{+/+} and *PDI*^{-/-} hMSCs upon addition of 2 mM DTT for 20 min, followed by addition of 100 μ M H₂O₂. Right, statistical analysis of the fluorescence intensity ratio at 500/400 nm excitation of HyPer-nucleus probe at 20 min post-DTT addition. *n* = 3 independent experiments.
- M Confocal imaging of *PDI*^{+/+} and *PDI*^{-/-} hMSCs expressing HyPer7-nucleus at steady state and upon addition of 2 mM DTT. The fluorescence intensity ratio at 488/405 nm obtained from individual cells was calculated at indicated times with a representative false color image. Scale bar, 10 μ m.
- Data information: In (B–F, L), data are presented as mean \pm SEM, two-tailed Student's *t*-test.
Source data are available online for this figure.

system (Ramming et al, 2014). At the resting state, the HyPer7-nucleus probe was mainly in its reduced state in both *PDI*^{+/+} and *PDI*^{-/-} hMSCs, indicating that the nucleus was harboring a low level of H₂O₂. Notably, HyPer7-nucleus in the *PDI*^{+/+} hMSCs responded to DTT challenge in a dose-dependent manner, whereas the probe in the *PDI*^{-/-} hMSCs was not oxidized at all (Fig 3K). HyPer7-nucleus in both cell lines was fully oxidized when exogenous H₂O₂ was added, suggesting that the probe was active (Fig 3L). Live imaging with confocal microscopy confirmed the abovementioned results at the single-cell level, which clearly showed that the nucleus was flooded with H₂O₂ upon DTT challenge, while PDI deletion abrogated this effect (Fig 3M). Similar results were observed when HyPer7 was targeted to the cytosol, although the probe was oxidized to a lesser extent, probably due to the powerful antioxidant system in the cytosol (Fig EV3H–J). These results suggest that the H₂O₂ generated by oxidative protein folding

can be efficiently released into the nucleus and cytosol and that knocking out PDI diminishes the release of ER-derived H₂O₂.

PDI deficiency attenuates cell senescence through the downregulation of SERPINE1 expression

To determine changes in gene expression during PDI-regulated cell senescence, we performed genome-wide RNA sequencing (RNA-Seq; Fig 4A). High reproducibility of transcriptome expression profiles between replicates was confirmed by principal component analysis (PCA) and measurements of Euclidean distance (Figs 4B and EV4A). By performing differential expression analysis, we identified 607 and 1,001 differentially expressed genes (DEGs) in early-passage (EP) and late-passage (LP) hMSCs, respectively (Fig EV4B and C). The RNA-Seq results also revealed that PDI deficiency partially restored the expression of DEGs in LP hMSCs to that in EP hMSCs

Figure 4. Deficiency of PDI alleviates cell senescence through downregulation of SERPINE1 expression.

- A Work flow for the RNA-Seq and proteomic analysis.
- B Principal component analysis (PCA) of transcriptome of early-passage (EP) and late-passage (LP) *PDI*^{+/+} and *PDI*^{-/-} hMSCs.
- C, D Density plots showing that upregulated (C) or downregulated (D) genes in the LP hMSCs (*PDI*^{+/+}, LP vs. *PDI*^{+/+}, EP) that were restored after PDI deletion (*PDI*^{-/-}, LP vs. *PDI*^{+/+}, LP). Comparisons were performed with two-sided Wilcoxon signed-rank test.
- E, F Heatmap showing upregulated (E) or downregulated (F) genes in the LP hMSCs (*PDI*^{+/+}, LP vs. *PDI*^{+/+}, EP) that were restored after PDI deletion (*PDI*^{-/-}, LP vs. *PDI*^{+/+}, LP). Representative GO terms, pathways and genes are shown on the right.
- G Volcano plots showing differentially expressed proteins (DEPs) between *PDI*^{-/-} and *PDI*^{+/+} hMSCs at LP.
- H Correlation analysis of the expression changes at the proteomic and transcriptional levels.
- I, J Heatmaps showing the upregulated (I) or downregulated (J) genes in the LP hMSCs (*PDI*^{+/+}, LP vs. *PDI*^{+/+}, EP) that were restored after PDI deletion at both the proteomic and transcriptional levels (*PDI*^{-/-}, LP vs. *PDI*^{+/+}, LP). Genes marked red represent the aging-related genes from "Aging Atlas" database (<https://ngdc.cnbc.ac.cn/aging>). The list of rescued genes was ranked based on Log₂ (fold change) in corresponding comparison.
- K Conjoint analysis showing the secretion levels of PDI and those in (I) and various SASPs from multiple senescence inducers and in plasma proteome from 3,087 healthy individuals (Basisty et al, 2020; Ritchie et al, 2021). RS, replicative senescence (*PDI*^{+/+}, LP vs. *PDI*^{+/+}, EP). ATV, atazanavir treatment; RAS, inducible RAS overexpression; IR, X-irradiation. The color keys that change from dark blue to dark purple represent the fold change of gene and protein, change from white to red represent the change in protein levels per unit increase in the covariate in plasma proteomic.
- L Dot plots showing the upregulated expression of *SERPINE1* in different human tissues during aging. These tissue-specific gene expression data were obtained from Genotype-Tissue Expression Project (GTEx). Red dots represent significantly upregulated expression in corresponding age groups (*P* < 0.05). Comparisons were performed with two-sided Wilcoxon rank-sum test.

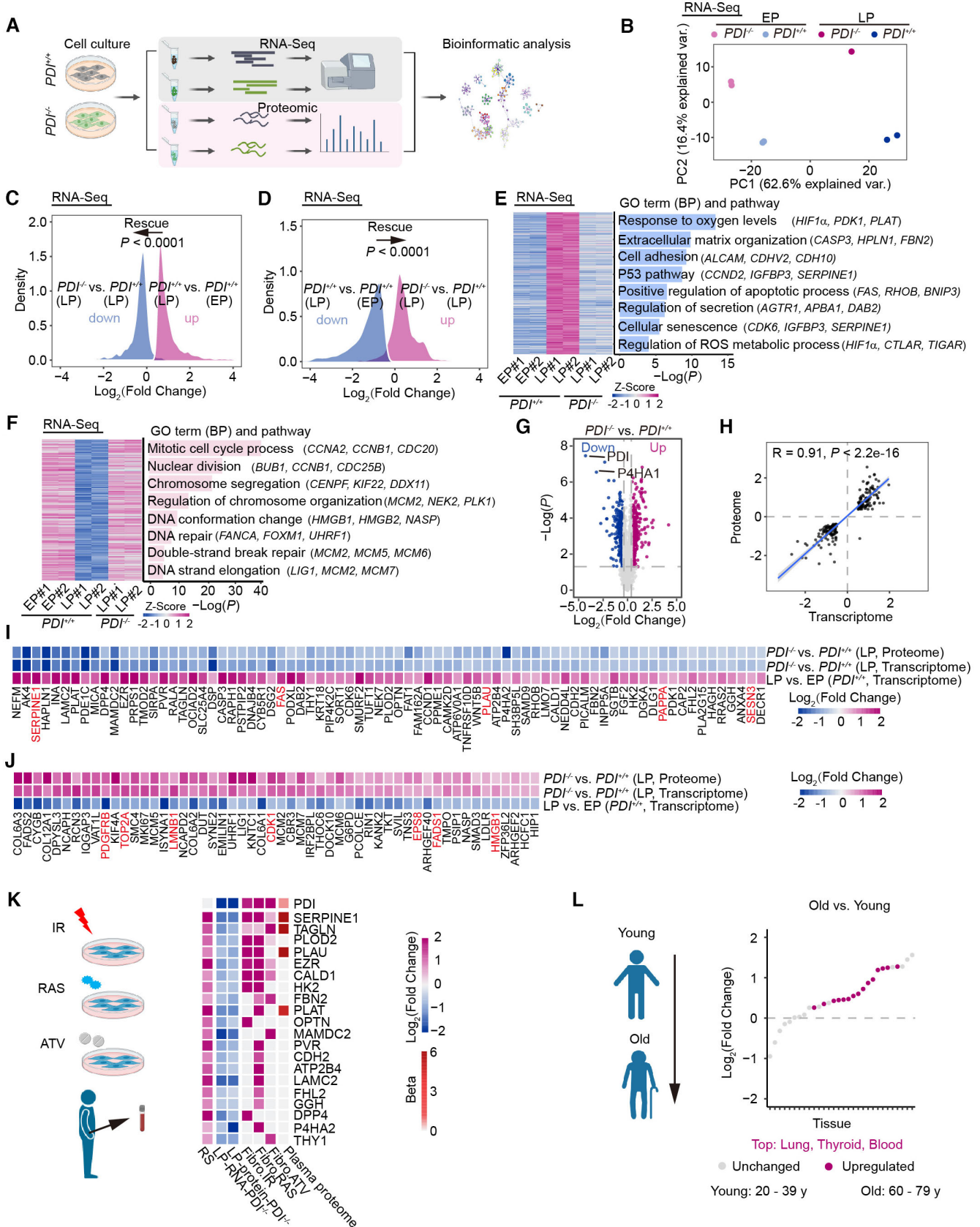


Figure 4.

(Fig 4C and D). A biology pathway analysis showed that DEGs enriched in “response to oxygen levels,” “P53 pathways,” “cellular senescence,” and “regulation of ROS metabolic process” were upregulated during cell senescence and downregulated by *PDI* depletion. In contrast, DEGs enriched in “mitotic cell cycle process” and “DNA repair” that had been downregulated during cell senescence were reactivated by *PDI* deletion (Fig 4E and F).

We next performed quantitative proteomic analysis of LP *PDI*^{+/+} and *PDI*^{-/-} hMSCs to identify changes in protein levels mediated by *PDI* knockout (Fig 4A and G). PCA and Euclidean distance measurements showed high reproducibility between replicates (Fig EV4D and E). In line with the results of RNA-Seq, we found that differentially expressed proteins (DEPs) and DEGs enriched in pathways such as “cell cycle,” “DNA replication,” and “DNA repair” were upregulated in the *PDI*^{-/-} hMSCs. In contrast, DEPs and DEGs enriched in pathways such as “response to oxygen levels” and “response to oxidative stress” were downregulated in the *PDI*^{-/-} hMSCs, consistent with results showing that deletion of *PDI* reduced H₂O₂ levels. In addition, “aging”-related DEGs and DEPs were downregulated, consistent with the phenotypes observed in the *PDI*^{-/-} hMSCs (Fig EV4F–I).

To better explore the molecular mechanisms of *PDI*-regulated cell senescence, we performed an integrated analysis with transcriptomic and proteomic data. A correlation analysis of DEGs and DEPs showed high congruence ($R = 0.91$, Fig 4H) between the transcriptomic and proteomic data. We further identified and ranked genes with expression that changed at both the transcriptional and proteomic levels. The analysis revealed 54 upregulated and 77 downregulated DEPs/DEGs in RS hMSCs, and the expression of these genes was reversed by *PDI* deletion (Fig EV4J and K). Moreover, after *PDI* deletion, the restored DEGs and DEPs were mainly enriched in “mitotic cell cycle,” “DNA repair,” “response to oxygen levels,” and “cellular senescence” terms (Fig EV4L and M). Next, we performed an integrative comparative analysis between the restored genes and

annotated hotspot aging-related genes obtained from an Aging Atlas gene set (Aging Atlas, 2021) and found that 12 of the restored genes were also hotspot aging-related genes (Fig 4I and J). Among these 12 genes, *SERPINE1* was found to be a key candidate with the greatest degree of recovery. In addition, in line with the expression of *PDI*, *SERPINE1* is a component in the SASP and a prominent plasma biomarker of aging (Fig 4K), underlining the potential correlation between dysregulation of *SERPINE1* and *PDI* expression during aging. Moreover, by analyzing the transcriptome profile of human tissues in different age groups, we found that the expression of *SERPINE1* was upregulated in most aged human tissues, such as the lung, thyroid, and blood (Fig 4L), implying that *SERPINE1* is closely related with physiological aging. Notably, *SERPINE1* is also a redox-regulated gene (Swiatkowska et al, 2002; Oszejca et al, 2008). Therefore, we reasoned that *PDI*-H₂O₂-*SERPINE1* may constitute a key axis that regulates stem cell aging.

***SERPINE1* is a key driver of cell senescence**

The *SERPINE1* gene encodes plasminogen activator inhibitor-1 (PAI-1), which negatively regulates the activities of two plasminogen activators (tissue-type PA, tPA, and urokinase-type PA, uPA) and therefore inhibits fibrinolysis (Rahman & Krause, 2020). In addition, PAI-1 plays an important role in regulating cell death, cell senescence and inflammation (Rahman & Krause, 2020). The mRNA and protein levels of *SERPINE1* were increased in senescent hMSCs, and this increase was not evident in *PDI*^{-/-} hMSCs (Fig 5A and B). To determine whether the geroprotective effect conferred by *PDI* deletion was due to the downregulation of *SERPINE1* expression, we induced the expression of *SERPINE1* in *PDI*^{-/-} hMSCs using a CRISPR/dCas9 transcriptional activation system (Joung et al, 2017; Fig 5C). The endogenous activation efficiency of two guide RNAs (gRNAs) targeting the promoter region of the *SERPINE1* gene was validated by western blotting (Fig 5D). Activation of endogenous

Figure 5. *PDI*-H₂O₂-*SERPINE1* axis plays a key role in cell senescence.

- A qPCR analysis of *SERPINE1* expression in *PDI*^{+/+} and *PDI*^{-/-} hMSCs at EP and LP. $n = 3$ independent experiments.
- B Western blotting analysis of *SERPINE1* protein in *PDI*^{+/+} and *PDI*^{-/-} hMSCs at EP and LP. GAPDH was used as the loading control of cell lysates. Ponceau was used as the loading control of conditional medium.
- C Schematic of CRISPR/dCas9 mediated transcriptional activation systems.
- D Western blotting of *SERPINE1* protein in *PDI*^{-/-} hMSCs transduced with two *SERPINE1*-targeting activation sgRNAs or sgNTC. GAPDH was used as the loading control.
- E Single clonal formation assay in *PDI*^{-/-} hMSCs transduced with sgNTC or *SERPINE1*-targeting activation sgRNAs. $n = 3$ biological repeats.
- F Left, Ki67 staining in *PDI*^{-/-} hMSCs transduced with sgNTC or *SERPINE1*-targeting activation sgRNAs. Scale bar, 20 μ m. Right, statistical analysis of Ki67-positive cells. $n = 3$ independent experiments.
- G Left, SA- β -gal staining in *PDI*^{-/-} hMSCs transduced with sgNTC or *SERPINE1*-targeting activation sgRNAs. Scale bar, 200 μ m. Right, statistical analysis of SA- β -gal-positive cells. $n = 3$ biological repeats.
- H qPCR analysis of the *SERPINE1* mRNA expression in *PDI*^{+/+} and *PDI*^{-/-} hMSCs treated with the indicated concentration H₂O₂ for 4 days. $n = 3$ independent experiments.
- I Left, western blotting analysis of the *SERPINE1* protein expression in *PDI*^{+/+} and *PDI*^{-/-} hMSCs treated with the indicated concentration H₂O₂ for 4 days. GAPDH was used as the loading control. Right, statistical analysis of relative *SERPINE1* protein levels. $n = 3$ independent experiments.
- J H₂O₂ levels in *PDI*^{-/-} hMSCs transduced with lentiviruses expressing Luc or *PDI* were determined by the fluorescence ratio of HyPer-ER at 488/405 nm excitation after the addition of 0.5 mM DTT for 15 min. $n = 3$ biological repeats.
- K H₂O₂ levels in *PDI*^{-/-} hMSCs transduced with lentiviruses expressing Luc or *PDI* were determined by the fluorescence ratio of HyPer7-nucleus at 500/400 nm excitation after the addition of 2 mM DTT for 20 min. $n = 3$ independent experiments.
- L Confocal imaging of *PDI*^{-/-} hMSCs transduced with lentiviruses expressing Luc or *PDI* and Hyper7-nucleus at steady state and upon addition of 2 mM DTT. The fluorescence intensity ratio at 488/405 nm obtained from individual cells was calculated at indicated times with a representative false color image. Scale bar, 10 μ m.
- M Western blotting of *SERPINE1* expression in *PDI*^{-/-} hMSCs transduced with lentiviruses expressing Luc or *PDI*. GAPDH was used as the loading control.

Data information: In (A, E–K), data are presented as mean \pm SEM, two-tailed Student's *t*-test.

Source data are available online for this figure.

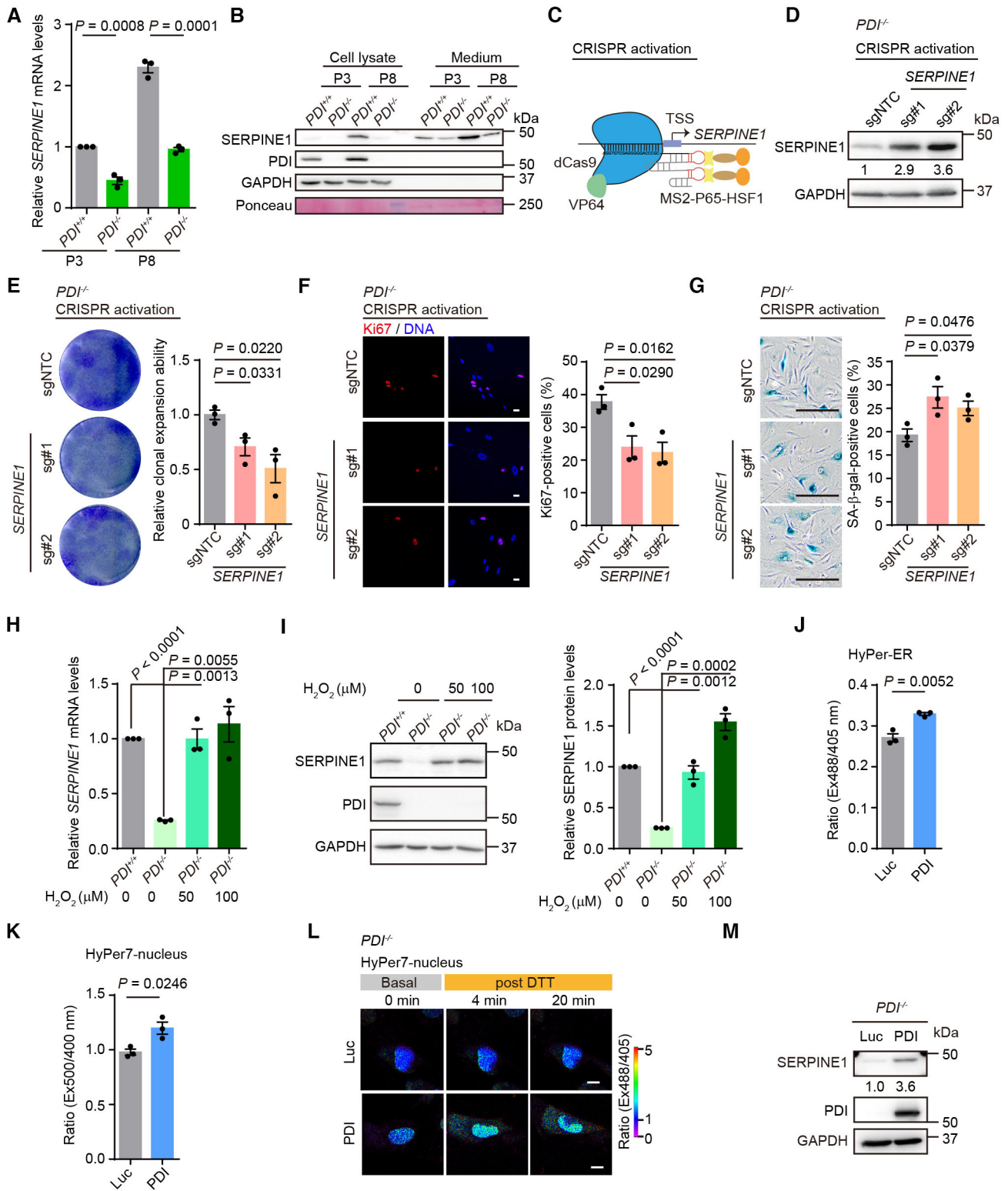


Figure 5.

SERPINE1 expression in *PDI*^{-/-} hMSCs accelerated cell senescence, as manifested by decreased single clonal formation ability, fewer Ki67-positive cells and increased SA-β-gal-positive cells (Fig 5E–G).

Moreover, the activation of *SERPINE1* expression in *PDI*^{+/-} hMSCs accelerated cell senescence (Fig EV5A–C), suggesting that *SERPINE1* is a driving force that mediates cell aging.

The PDI-H₂O₂ axis regulates SERPINE1 expression

Next, we wondered whether the expression of SERPINE1 was mediated by H₂O₂ levels. The addition of H₂O₂ increased both the transcriptional and protein levels of SERPINE1 in *PDI*^{-/-} hMSCs to an extent similar to those in *PDI*^{+/+} hMSCs (Fig 5H and I). Importantly, the same concentration of H₂O₂ induced the senescence of *PDI*^{-/-} hMSCs (Fig EV5D and E). Furthermore, reintroduction of *PDI* into *PDI*^{-/-} hMSCs increased the H₂O₂ levels in the ER (Fig 5J) and enhanced the release of H₂O₂ into the nucleus (Fig 5K and L) and cytosol (Fig EV3K and L). Replenishment of *PDI* also led to the upregulated expression of SERPINE1 (Fig 5M). Therefore, we conclude that PDI regulates the expression of SERPINE1 via H₂O₂ and that PDI-H₂O₂-SERPINE1 axis constitutes an important pathway that contributes to cell senescence.

Targeting PDI alleviates senescence in diverse cell types

To explore the geroprotective role of *PDI* depletion in a wider range of cell types, RS hMSCs, premature-senescent hMSCs (Hutchinson-Gilford Progeria Syndrome, HGPS; and WS hMSCs), and primary hMSCs from an elderly individual were edited via CRISPR/Cas9 technology to knockdown *PDI* expression (Fig 6A). In all the hMSCs models, *PDI* knockdown alleviated cell senescence, as manifested by increased clonal expansion ability and a decreased percentage of SA-β-gal-positive cells (Fig 6B and C). Moreover, *PDI* knockdown mitigated wild-type hMSCs senescence induced by different cellular stressors, including ultraviolet radiation (UV) and oncogene overexpression (Fig 6D–G). Additionally, *PDI* knockdown inhibited the senescence of human fibroblasts (Fig EV5F–H). Altogether, these results indicate that *PDI* is a potential target for alleviating cell senescence in different types of hMSCs and human fibroblasts.

Discussion

In this study, we established a novel link between oxidative protein folding and cell aging. We observed that the expression of PDI, a key enzyme catalyzing disulfide bonds formation in the ER, was upregulated during replicative and premature hMSCs senescence. Increased PDI accelerated oxidative protein folding, resulting in the accumulation of the byproduct H₂O₂ in both the ER and nucleus.

ER-derived oxidative stress induced the expression of SERPINE1, which promoted cell senescence furtherly (Fig 6H).

Since PDI is widely considered to be important for disulfide bonds formation and *PDI*-knockout mice are embryonic lethal (Xu et al, 2014; Parakh & Atkin, 2015), the viability of *PDI*-knockout hMSCs is surprising. Moreover, they were healthier and younger than wild-type cells. The high redundancy of PDI family proteins in the ER may explain this outcome. We showed that the recombination of four PDI homologs, namely ERp57, P5, ERp72, and ERp46, led to disulfide formation in cooperation with Ero1α oxidase, but the oxygen consumption and H₂O₂ production rates were slower than with PDI. In addition, the rate of oxidative folding of the J-chain in *PDI*^{-/-} hMSCs was slowed, and fewer high-molecular-weight species due to indiscriminate oxidation by H₂O₂ accumulated (Wang et al, 2014). Moreover, *PDI* knockout attenuated the upregulated expression of Ero1α during aging, further lowering the risk of oxidative stress. Thus, *PDI* deletion resulted in slower but safer oxidative protein folding in hMSCs. However, this outcome does not mean that PDI is dispensable in all developmental stage and all types of cells. For example, the *PDI* knockout mice have lethal phenotypes occurring at E9.5 (<https://www.mousephenotype.org/data/genes/MGI:97464>), which is later than the blastocyst-stage where the hESCs derived, and *PDI*^{-/-} hESCs cannot be differentiated into human vascular endothelial cells (hVECs) efficiently (our unpublished observation), suggesting that PDI may play an important role in angiogenesis. Besides, in pancreas β-cells, PDI is required for the correct disulfide formation of proinsulin (Jang et al, 2019). In addition, PDI associates with Drp1 to protect endothelial cells against mitochondrial fragmentation and endothelial dysfunction (Kim et al, 2018).

According to the free radical theory of aging, accumulating ROS induce oxidative stress and promote cell senescence (Harman, 1956; Kudryavtseva et al, 2016). Yet, previous studies of oxidative stress on cell senescence have mostly focused on mitochondrion-derived ROS (Li et al, 2013; Vasileiou et al, 2019), the role of ER-generated ROS has been less extensively studied. In fact, the ER may be the most significant ROS producer in some cell types, and among purified organelles, ER-derived ROS accounts for approximately 60% of all the ROS produced (Colton & Gilbert, 2007). Previous results have shown that upregulation of Ero1 resulted in excessive ROS production, while knockdown of Ero1 reduced the peroxide levels in worms, extending their lifespan by 32% (Curran & Ruvkun, 2007). Ero1-generated H₂O₂ can be eliminated by ER-resident glutathione

Figure 6. Targeting PDI alleviates senescence in diverse cell types.

- A Western blotting of PDI expression in replicative senescent (RS) hMSCs, Hutchinson-Gilford Progeria Syndrome (HGPS) hMSCs, WS hMSCs and human primary hMSCs from an old individual transduced with sgNTC or *PDI*-targeting sgRNA. GAPDH was used as the loading control.
- B Single clonal formation assay in RS hMSCs, HGPS hMSCs, WS hMSCs and human primary hMSCs from an old individual transduced with sgNTC or *PDI*-targeting sgRNA. *n* = 3 biological repeats.
- C SA-β-gal staining in RS hMSCs, HGPS hMSCs, WS hMSCs and human primary hMSCs from an old individual transduced with sgNTC or *PDI*-targeting sgRNA. *n* = 3 biological repeats. Scale bar, 200 μm.
- D–G (D, F) Single clonal formation assay (D) and SA-β-gal staining assay (F) in RS hMSCs transduced with sgNTC or *PDI*-targeting sgRNA after treatment with UV irradiation (10 J/m²) and then cultured for another 2 days. *n* = 3 biological repeats. (E, G) Single clonal formation assay (E) and SA-β-gal staining assay (G) in RS hMSCs transduced with sgNTC or *PDI*-targeting sgRNA after overexpressing of H-Ras^{V12}. *n* = 3 biological repeats. Scale bar, 200 μm.
- H A model showing PDI and its upstream oxidase Ero1α are upregulated during aging, and Ero1α-PDI mediated oxidative protein folding produces excess H₂O₂ in the ER as well as in the nucleus, upregulates the expression of SASP including SERPINE1, disrupts hMSCs homeostasis and promotes senescence.

Data information: In (B–G), data are presented as mean ± SEM, two-tailed Student's *t*-test. Source data are available online for this figure.

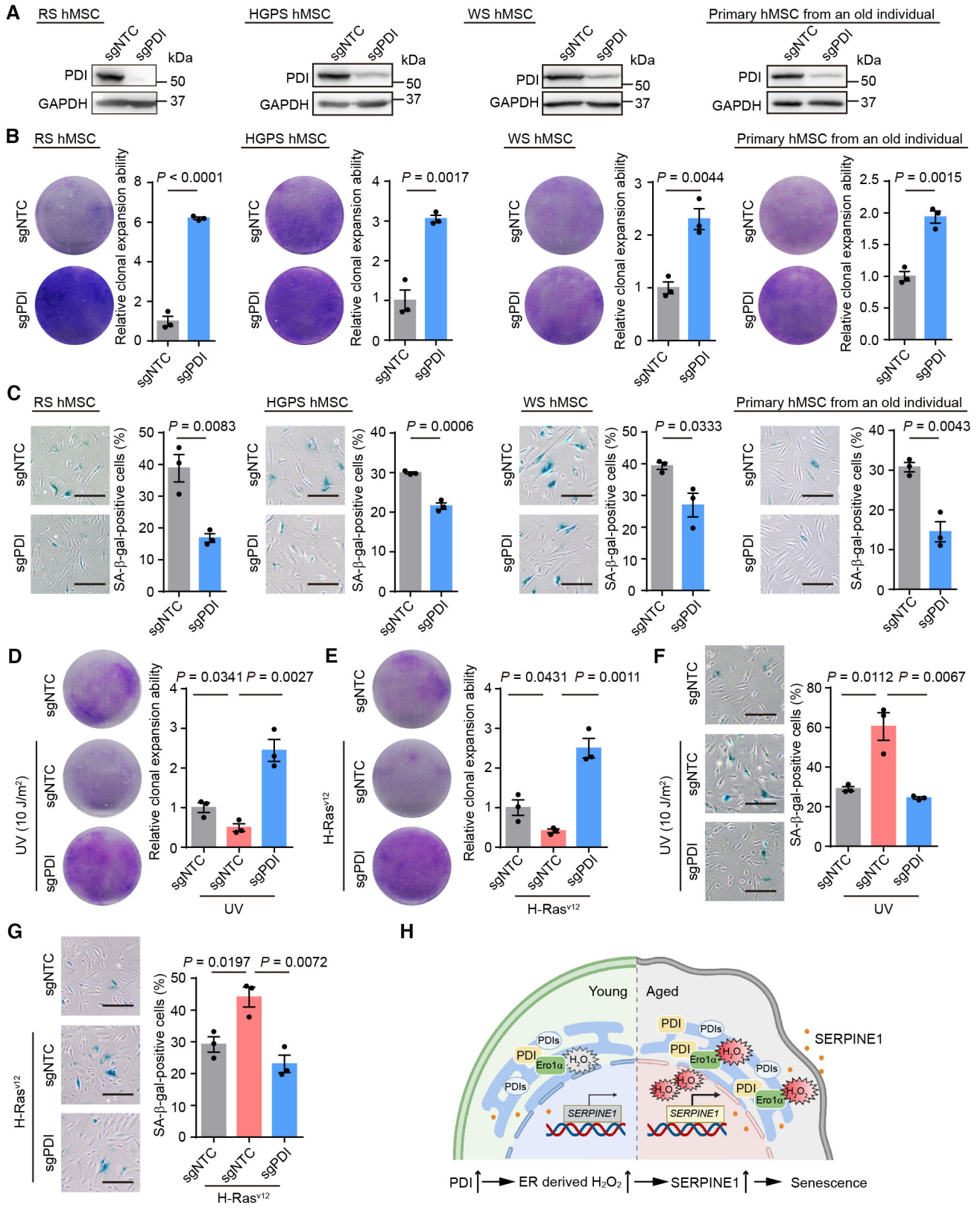


Figure 6.

peroxidase 7 (GPx7; Wang et al, 2014). Our previous study showed that GPx7 knockdown promoted cell senescence (Fang et al, 2018), further emphasizing the role played by ER-derived H₂O₂ in aging. However, whether H₂O₂ can readily pass through the ER membrane and affect other organelles has been contentiously debated (Konno et al, 2015; Appenzeller-Herzog et al, 2016). In this study, by using the ultrasensitive H₂O₂ probe HyPer7, we clearly showed that the H₂O₂ generated by oxidative protein folding was released into the nucleus and cytosol. As a mobile signaling molecule, H₂O₂ can participate in the regulation of gene expression during stem cell aging (Barandalla et al, 2017). How the H₂O₂ generated in the ER is released into the nucleus or cytosol remains unclear. One candidate is ER membrane-localized aquaporin 11 (AQP11), as indicated by downregulation of AQP11 severely disrupting the flux of H₂O₂ through the ER (Appenzeller-Herzog et al, 2016; Basisty et al, 2020).

The lack of an animal or a cell model has largely limited the investigation of PDI and oxidative protein folding in the regulation of aging. In this study, we established PDI-knockout hESCs and showed that *PDI*^{-/-} hESCs maintained pluripotency and self-renewal capacity. In addition, *PDI*^{-/-} hESCs were differentiated into hMSCs. Thus, our study provides valuable cell models for exploring the biological function of PDI in various human stem cells and a potential strategy for generating genetic enhancement human stem cells for cell therapies. The geroprotection conferred by *PDI* depletion was validated in various types of hMSCs and human fibroblasts. The unexpected function of PDI in regulating cell senescence highlights PDI as a newly discovered potential target for alleviating aging. Recently, PDI has emerged as a potential target for cancer and thrombosis treatment (Xu et al, 2014; Bekendam & Flaumenhaft, 2016; Wang et al, 2021). It will be interesting to investigate whether anticancer and antithrombotic PDI inhibitors can be used for aging intervention.

Furthermore, we revealed that the redox and aging-related gene *SERPINE1* is regulated by the PDI-H₂O₂ axis and functions as a key driver of cell senescence. *SERPINE1* is regarded as a vital component of the senescence-related secretome (Khan et al, 2017). In line with previous reports indicating that *SERPINE1* expression is regulated via H₂O₂ (Swiatkowska et al, 2002; Osza jca et al, 2008), our study indicated that exogenous H₂O₂ or ER-derived H₂O₂ promoted the expression of *SERPINE1*, which further accelerated cell senescence. Therefore, it is likely that the leaked H₂O₂ from the ER during oxidative protein folding activates oxidative stress-related transcription factors such as NF-κB and HIF-1 in the nucleus, and upregulates *SERPINE1* gene expression (Osza jca et al, 2008; Rahman & Krause, 2020). Since it is a secretory protein, *SERPINE1* can be used as a reliable and convenient biomarker of aging. Moreover, as both PDI (Kim et al, 2013; Wang et al, 2022c) and *SERPINE1* (Westrick & Eitzman, 2007; Hisada et al, 2021) have been well-documented to be associated with thrombosis, targeting the PDI-H₂O₂-*SERPINE1* axis may be a more effective strategy for the prevention and treatment of vascular disease.

Materials and Methods

Cell culture

PDI^{+/+} hESCs (Line H9, WA09, WiCell Research Institute, Inc.) and *PDI*^{-/-} hESCs were cultured on Mitomycin C (MMC; Selleck)-inactivated mouse embryonic fibroblast (MEF) feeder cells in the

hESCs culture medium supplemented with DMEM/F12 medium (Gibco), 20% KnockOut Serum Replacement (Gibco), 2 mM GlutaMAX (Gibco), 0.1 mM nonessential amino acids (NEAA, Gibco), 100 μg/ml streptomycin and 100 U/ml penicillin (Thermo Fisher Scientific), 55 μM β-mercaptoethanol (Thermo Fisher Scientific), and 10 ng/ml FGF2 (Joint Protein Central, JPC) or on Matrigel (Corning) in mTeSR medium (STEMCELL Technologies). hMSCs were cultured in 0.1% Gelatin-coated plates in hMSC medium containing α-MEM basal medium (Gibco), 10% fetal bovine serum (FBS, Gibco), 0.1 mM NEAA (Gibco), 100 μg/ml streptomycin and 100 U/ml penicillin (Thermo Fisher Scientific), and 1 ng/ml FGF2 (JPC). Human fibroblasts (BJ-1, ATCC) and HEK293T cells were cultured in high-glucose DMEM (Thermo Fisher Scientific) supplemented with 10% FBS and 100 μg/ml streptomycin and 100 U/ml penicillin. There was no mycoplasma contamination observed during cell culture.

Generation of *PDI*^{-/-} hESCs

The *PDI* gene knockout was performed with the CRISPR/Cas9 genome editing system (Hu et al, 2020; Zhang et al, 2022a). In brief, the guide sequence targeting the exon 2 of the *PDI* gene was cloned into the pCAG-mCherry-gRNA vector (Addgene #87110). H9 hESCs were cultured in Matrigel-coated plates in mTeSR medium and were pretreated with the ROCK inhibitor Y-27632 (Selleck) for 24 h before plasmid electroporation. The H9 hESCs were dissociated with TrypLE (Thermo Fisher Scientific), and 5 × 10⁶ H9 ESCs were electroporated with 14 μg pCAG-1BP-NLS-Cas9-1BP-NLS-2AGFP (Addgene #87109) vectors and 7 μg pCAGmCherry-PDI-gRNA vectors using a 4D Nucleofector (Lonza). After 48 h culture in mTeSR medium, GFP and mCherry double-positive cells were sorted by FACS (BD, Aria II) and then cultured on MMC-inactivated MEF cells in hESC culture medium. After 2 weeks in culture, emerging colonies were picked into a 24-well culture plate and expanded for genomic DNA extraction and sequencing identification.

The sequence for the *PDI* guide RNA (gRNA) was 5'-GCGAAAAGCAACUUCGCGG-3'. The primers for clone identification were 5'-CAGGATTTATAAAGGCGAGGC-3' (forward) and 5'-CTCACAGAACTCCACCAGCA-3' (reverse).

Generation and characterization of *PDI*^{+/+} and *PDI*^{-/-} hMSCs

Differentiation of hESCs into hMSCs was performed as described previously (Cheng et al, 2019; Shan et al, 2022). Briefly, embryoid bodies (EBs) were derived from hESCs and plated onto Matrigel-coated plates in hMSC differentiation medium containing 90% α-MEM, 10% FBS, 0.1 mM NEAA, 100 μg/ml streptomycin and 100 U/ml penicillin, 10 ng/ml FGF2 (JPC) and 5 ng/ml TGFβ (HumanZyme). After about 10 days, the fibroblast-like cells appeared. The cells were then transferred into gelatin-coated plates in hMSC culture medium. Then, CD73, CD90, and CD105 tri-positive cells were sorted as hMSCs by FACS (BD, Aria II). Identification of hMSC-specific markers with antibodies including anti-human CD73-PE (BD, 550257), anti-human CD90-FITC (BD, 555595), and anti-human CD105-APC (BD, 323208). CD43, CD34, and CD45 were used as negative markers for verifying hMSCs by FACS (BD FACS Calibur). Negative hMSC markers with antibodies including anti-human CD34-FITC (BD, 555821), anti-human CD43-APC (BD,

560198), and anti-human CD45-FITC (BD, 555482). To evaluate the multiple-lineage differentiation abilities, differentiation of hMSCs toward chondrocytes, osteoblasts, and adipocytes and characterized by Toluidine blue (Sigma, 89,640, chondrogenesis), Alizarin Red S staining (Sigma, A5533, osteogenesis), and Oil red O (Sigma, O1391, adipogenesis) staining.

Isolation and culture of primary hMSCs

The primary hMSCs were isolated from a 76-year-old healthy male gingiva tissues according to previous report (Hu *et al.*, 2020; He *et al.*, 2022). Briefly, the gingiva tissues were cut into granule and digested in TrypLE (Thermo Fisher Scientific) and Dispase IV (Thermo Fisher Scientific) at 37°C for 30 min. Then, the digested tissues were filtered through a 70- μ m cell strainer (Falcon) and centrifuged at 500 g for 10 min. The pellets were cultured in the hMSCs culture medium for about 14 days in gelatin-coated plates. Primary hMSCs were isolated from the dental pulp tissues of different individuals with the approval from the Ethics Committee of the 306 Hospital of PLA in Beijing (Ren *et al.*, 2019).

Copy number variation (CNV) identification

The genomic DNA from hESCs or hMSCs was extracted using a DNeasy Blood & Tissue Kit (TIANGEN). To obtain DNA fragments of approximately 300 base pairs, the extracted genomic DNA was subjected to ultrasonication by Covaris. Sequencing libraries were constructed with the Next DNA Library Prep Reagent Set for Illumina (NEB). WGS data analysis was performed as previously described (Liu *et al.*, 2022b). In brief, we trimmed raw reads with TrimGalore. Then, the clean reads were mapped to the human hg19 genome. The mapped reads were further filtered using samtools and Picard software. Remained reads were counted for each 500-kb window using read counter function in HMMcopy_utils (https://github.com/shahcompbio/hmmcopy_utils). The R/Bioconductor package HMMcopy (v1.26.0) was used to correct copy number, GC content and mappability.

Clonal expansion assay

Clonal expansion assay was performed as described previously (Liang *et al.*, 2021; Lei *et al.*, 2022; Zhao *et al.*, 2022). In brief, about 2,000 cells were seeded on a 12-well plate coated with gelatin. Approximately 10 days later, the cells were washed with PBS, fixed with 4% paraformaldehyde (PFA) at room temperature for 30 min, and stained with 0.1% crystal violet solution (Sigma) at room temperature for 30 min. After wash with water, images were captured by Epson Perfection V370 Photo and relative cell density was quantified using ImageJ.

Senescence-associated β -galactosidase (SA- β -gal) staining

SA- β -gal staining assay was carried out as described previously (Ren *et al.*, 2019; Hu *et al.*, 2020; Liu *et al.*, 2023). In brief, hMSCs on six-well plates were washed with PBS twice, and then fixed in fixation buffer containing 2% (w/v) formaldehyde and 0.2% (w/v) glutaraldehyde for 5 min at room temperature. After that, cells were washed with PBS twice and stained with SA- β -gal staining buffer

containing 5 mM $K_4[Fe(CN)_6]$, 5 mM $K_3[Fe(CN)_6]$, 150 mM NaCl, 2 mM $MgCl_2$, 40 mM citric acid/Na phosphate buffer, 1 mg/ml X-gal (AMRESCO) at 37°C overnight. Stained cells were then captured with a digital microscope camera (Olympus) and the number of SA- β -gal-positive cells was quantified by ImageJ.

Animal experiments

All animal experiments conducted in this research were approved by the Institutional Biomedical Research Ethics Committee of the Institute of Biophysics and Institute of Zoology, CAS. The mice were raised and housed at 25°C in the Laboratory of Immunodeficiency Animals of Institute of Biophysics and Institute of Zoology, CAS, on a 12-h light–dark cycle. For the western blotting assay, C57BL/6J male mice (SiPeiFu) were euthanized and tissues were collected. For the teratoma assay, hESCs were harvested in a Matrigel/mTeSR (1:4) solution and the mixtures were injected into the inguinal region of NOD/SCID mice (male, 4–6 weeks, GemPharmatech). After about 2 months, the teratomas were collected and analyzed using immunofluorescence staining. The hMSC transplantation assay was carried out as previously described (Bi *et al.*, 2020). Briefly, about 1×10^6 hMSCs expressing luciferase were injected into the tibialis anterior (TA) muscle of nude mice (male, 6–8 weeks, GemPharmatech). The luciferase activity of mice was imaged using IVIS spectrum imaging system (XENOGEN, Caliper) every 2 days after injection.

Immunofluorescence microscopy

Immunostaining was conducted as described previously (Shan *et al.*, 2022; Wang *et al.*, 2022d). Briefly, cells on the coverslips were washed twice with PBS and fixed with 4% PFA at room temperature for 15 min, washed with PBS twice, and permeabilized with 0.4% Triton X-100 in PBS at room temperature for another 5 min and then blocked with 10% donkey serum (Jackson ImmunoResearch Labs) in PBS at room temperature for 1 h. The cells were then incubated with primary antibodies in blocking solution at 4°C overnight and then incubated the corresponding fluorescent secondary antibodies in dark at room temperature for 1 h. Images were captured using a confocal microscope (Leica SP5 and Nikon). The primary antibodies used were as follows (company, catalog number): anti-OCT4 (Santa Cruz, sc-5279), anti-SOX2 (Santa Cruz, sc-17320), anti-NANOG (Abcam, ab21624), anti-Ki67 (ZSGB-Bio, ZM-0166), anti- γ H2AX (Millipore, 05–636), anti-53BP1 (Bethyl Laboratories, A300-273A), anti- β -tubulin III (TuJ1, Sigma, T2200), anti-SMA (Abcam, ab32575), anti-FOXA2 (Cell Signaling Technology, 8186S), anti-PDI (Abcam, ab2792), anti-calreticulin (Abcam, ab2907), and anti-LAP2 (BD, 611000).

Cell cycle analysis

Cell cycle analysis was performed as previously described (Zhang *et al.*, 2019b). Cells were harvested and washed twice with PBS, and then were fixed in 70% ethanol at -20°C overnight. The fixed cells were washed with PBS and stained with 200 μ L propidium iodide (Invitrogen) for 30 min in dark at room temperature. Samples were then analyzed by BD flow cytometry, and cell-cycle phase distributions were analyzed by the ModFit software.

Determination of cytosol, mitochondria, and ER redox states

$PDI^{+/+}$ and $PDI^{-/-}$ hMSCs were infected with PLE4-roGFP-cytosol, PLE4-roGFP-mitochondria or PLE4-roGFP-ER lentiviruses for 72 h, harvested and washed with Hanks' Balanced Salt Solution (HBSS, Gibco), and then transferred into a flat-bottom 96-well plates. For the roGFP-cytosol and roGFP-mitochondrial, the fluorescence intensity was measured at 525 nm with excitation at 405 and 488 nm using an EnSpire Multimode Plate Reader (Perkin Elmer), and the ratio of 405/488 nm was calculated. For the roGFP-ER, the fluorescence intensity was measured at 525 nm with excitation at 390 and 465 nm, and the ratio of 390/465 nm was calculated.

In vivo oxidative protein folding assays

The *in vivo* myc-tagged Ig-J chains (JcM) folding assay was performed as described (Zhang et al, 2018). In brief, $PDI^{+/+}$ and $PDI^{-/-}$ hMSCs transfected with pcDNA3.1-JcM for 48 h were harvested and incubated in MSC culture medium containing 5 mM DTT for 5 min at 37°C. The cells were washed twice with ice-cold PBS immediately, and then aliquoted and resuspended with fresh culture medium at 20°C. Aliquots were taken at different time points, quenched by 20 mM NEM on ice, and lysed in RIPA buffer containing protease inhibitor cocktail and 20 mM NEM for 30 min on ice. The supernatants were resolved by nonreducing SDS-15% PAGE and analyzed by western blotting. The *in vivo* Flag-tagged LDLR (1–236) folding assay was similar to the JcM folding assay.

Determination of H₂O₂ levels in the ER

The H₂O₂ levels in the ER were detected using HyPer-ER probe according to previous reports (Zhang et al, 2019b). In brief, hMSCs infected with PLE4-HyPer-ER for 72 h were washed twice with HBSS, and then transferred into a flat-bottom 96-well plates. The fluorescence intensity of the cells was measured at 530 nm with excitation at 405 and 488 nm for 5 min, and then for another 15 min in the presence of 0.5 mM DTT using an EnSpire Multimode Plate Reader. The ratio of 488/405 nm was calculated.

Determination of the release of H₂O₂ to the nucleus or cytosol

$PDI^{+/+}$ and $PDI^{-/-}$ hMSCs were infected with the viruses of PLE4-HyPer7-nucleus or PLE4-HyPer7-cytosol. 72 h later, the cells were harvested and resuspended with HBSS, and then transferred into a flat-bottom 96-well plates. The fluorescence intensities were measured at 520 nm with excitation at 400 and 500 nm using EnSpire Multimode Plate Reader for 5 min as steady state. To investigate the release of H₂O₂ in the ER, 0.5, 1 or 2 mM DTT was added into different wells and the fluorescence intensity was measured for about 30 min. At last, 100 μM H₂O₂ was added into the wells, and then the ratio of 500/400 nm was calculated.

For imaging experiments, $PDI^{+/+}$ and $PDI^{-/-}$ hMSCs were infected with the viruses of PLE4-HyPer7-nucleus or PLE4-HyPer7-cytosol and then were seeded into 35-mm glass bottom dishes. Cell imaging was performed using a Nikon confocal microscopy. Fluorescence of HyPer7 probes was excited sequentially via 405 and 488 nm and with 500–550 nm emission. After 2–4 images were

acquired, 2 mM DTT was added. The ratio images were calculated using the confocal software according to fluorescence intensity.

Lentivirus production

Lentivirus production was performed as previously described (Wu et al, 2020; Jing et al, 2022). Briefly, HEK293T cells were co-transfected with corresponding lentiviral vectors, psPAX2 (Addgene, #12260) and pMD2G (Addgene, #12259) using Lipofectamine™ 3000 Transfection Reagent (Thermo Fisher Scientific). Viral particles were collected by ultracentrifugation at 19,400 g for 2.5 h at 4°C.

Lentiviral CRISPR/Cas9-mediated gene knockout or CRISPR/dCas9-mediated gene activation

Lentiviral CRISPR/Cas9-mediated gene knockout and CRISPR/dCas9-mediated gene activation were performed as previously described (Wu et al, 2020; Sun et al, 2022a; Wang et al, 2022d). To construct CRISPR/Cas9-mediated gene knockout lentiviral vectors, the sgRNA targeting *PDI* was inserted in the lentiCRISPRv2 (Addgene, #52961). For knockout of the expression of *PDI*, hMSCs were transduced with Lenti-CRISPRv2-*PDI*. 48 h later, the cells were selected with puromycin (Invitrogen, ant-pr-1) for 7 days. CRISPRv2-NTC (nontargeting control) was used as negative control. The sequence of *PDI* sgRNA was 5'-AGGCAGAAGGUUCCGAGAUC-3'. To induce endogenous *SERPINE1* expression, sgRNA targeting the transcriptional start site (TSS) of *SERPINE1* was inserted into lentiSAM v2 vector (Addgene, #75112). LentiSAM v2-NTC (nontargeting control) was used as negative control. For the induction of endogenous expression of *SERPINE1*, hMSCs were co-transduced with the LentiSAM v2 and LentiMPH v2 (Addgene, #89308) to transcriptionally activate the expression of *SERPINE1*. 48 h later, the cells were selected with blasticidin (Sigma, 15205) and hygromycin (Invitrogen, ant-hg-1) for 7 days. The sequences of *SERPINE1* sgRNA were used as follows:

SERPINE1-sgRNA#1: 5'-UCCUCUCUGGGACUUGCUG-3',
SERPINE1-sgRNA#2: 5'-AGGUGUCGAGGGGACCCGC-3'.

Western blotting

Western blotting was performed as previously described (Liu et al, 2022a). Briefly, cells were lysed in lysis buffer (Millipore) containing phosphatase and protease inhibitor cocktail (Roche) for 30 min on ice. Then, cell lysates were centrifuged at 17,000 g for 30 min at 4°C, and protein concentration was determined by a BCA protein quantification kit. 20 μg sample was loaded and separated by SDS-PAGE and then transferred to PVDF membranes (Millipore). The membranes were then blocked in TBST buffer containing 5% (w/v) nonfat powdered milk for 1 h. Subsequently, the membranes were incubated with primary antibodies overnight at 4°C followed by HRP-conjugated secondary antibodies at room temperature for 1 h. The imaging was performed using a ChemiScope Mini imaging system (Clinx Science) with enhanced chemiluminescence (Thermo Fisher). The primary antibodies used for western blotting in this study were anti-*PDI* (Abcam, ab2792), anti-*SERPINE1* (Santa Cruz, sc-5297), anti-GAPDH-HRP (Sigma-Aldrich, G9295), anti-Myc (Sigma, M4439), anti-ERp44 (Cell Signaling Technology, #3798),

anti-ERp46 (Animal Facility, Institute of Genetics and Developmental Biology, CAS, rabbit serum), anti-ERp57 (Cell Signaling Technology, #2881), anti-ERp72 (OriGene, TA503904), P5 (PTM BIO, PTM-5512), anti-P4HA1 (PTM BIO, PTM-5859), anti-P4HA2 (PTM BIO, PTM-6033), anti-FLAG (Sigma, 220,616), P16 (BD, 550834), Ero1 α (Sigma-Aldrich, MAB T376).

H₂O₂ measurement in PDI^{+/+} and PDI^{-/-} hMSCs via Amplex red

The cellular H₂O₂ levels were quantified by Amplex Red Hydrogen Peroxide/Peroxidase Assay Kit (Invitrogen, A22188) according to the manufacturer's instructions. PDI^{+/+} and PDI^{-/-} hMSCs were harvested and lysed in lysis buffer on ice for 30 min. Then the cell lysates were centrifuged at 17,000 g for 10 min at 4°C, and the protein concentration was quantified by BCA Kit. Then, the same amount of protein of supernatants was transferred to a black 96-well plate. 50 μ M Amplex Red reagent and 0.1 U/ml horseradish peroxidase (HRP) in HBSS were added into each well and incubated at 37°C for 30 min. Fluorescence intensity was measured at 590 nm with excitation at 545 nm.

H₂O₂ measurement *in vitro*

To measure the production of H₂O₂ under different conditions, DTT-reduced PDI, ERp57, P5, ERp72, and ERp46 (10 μ M each) were mixed in 50 mM sodium phosphate buffer, pH 7.4 in a 96-well microtiter plate. Ero1 α (1 μ M) together with horseradish peroxidase (0.1 U/ml) and Amplex Red (5 μ M) were added to the PDI mixture to initiate H₂O₂ production. The production of H₂O₂ was monitored kinetically at 550 nm excitation and 590 nm emission for 30 min.

Oxygen consumption assay

Oxygen consumption was monitored using an Oxygraph Clark-type oxygen electrode (Hansatech Instruments) as previously described (Wang *et al*, 2011). Reactions were initiated by adding Ero1 α protein to a final concentration of 1 μ M into buffer B (100 mM Tris-HAc, pH 8.0, 50 mM NaCl, 2 mM EDTA) containing PDI, ERp57, P5, ERp72, and ERp46 proteins (10 μ M each) and 10 mM glutathione (GSH).

Measurement of cellular reactive oxygen species (ROS)

Cellular total ROS levels were measured using 2.5 μ M H₂DCFDA (Invitrogen, C6827), as previously reported (Diao *et al*, 2021). Cells were stained with H₂DCFDA for about 15 min at 37°C in the dark, and then analyzed by flow cytometry (BD).

ELISA analysis of the secretion of IL6

ELISA analysis of the secretion of IL6 was performed as previously described (Hu *et al*, 2020; Liu *et al*, 2023). Briefly, the supernatants from PDI^{+/+} and PDI^{-/-} hMSCs were collected and centrifuged at 500 g for 5 min. Then, the supernatants were incubated with IL6 antibody-coated ELISA plates according to the manufacturer's manual (BioLegend). Finally, the absorbance at 450 nm was detected using a Multimode Plate Reader and the data were normalized to cell numbers.

Telomere length analysis

Analysis of the telomere length by qPCR was performed as previously described (Zhang *et al*, 2019a). Briefly, the genomic DNA of PDI^{+/+} and PDI^{-/-} hMSCs was extracted using a DNeasy Blood & Tissue Kit (TIANGEN), and qPCR was performed to analyze the telomere length using the following primers. Telomere-36B4u was used as the internal reference.

Telomere-tel-F: 5'-GGTTTTTGAGGGTGAGGGTGAGGGTGAGGGTGAGGGT-3',

Telomere-tel-R: 5'-TCCCGACTATCCCTATCCCTATCCCTATCCCTATCCCTATCCCTA-3',

Telomere-36B4u-F: 5'-CAGCAAGTGGGAAGGTGTAATCC-3',

Telomere-36B4u-R: 5'-CCCATTCTATCATCAACGGGTACAA-3'.

RNA extraction and RT-qPCR

RNA extraction and RT-qPCR were performed as previously described (Bi *et al*, 2020). In brief, total RNA was extracted by TRIzol reagent (Invitrogen). 2 μ g of RNA was used for cDNA synthesis using the GoScript Reverse Transcription System (Promega). qPCR was performed using SYBR Select Master Mix (Thermo Fisher Scientific) on a QuantStudio 7 Flex machine (Applied Biosystems). The relative expression of genes was normalized to the GAPDH transcript. The qPCR primers used are as follows:

GAPDH forward primer, 5'-GGAGCGAGATCCCTCCAAAAT-3',

GAPDH reverse primer, 5'-GGCTGTTGTCATACTTCTCATGG-3',

SERPINE1 forward primer, 5'-ACCGCAACGTGGTTTTCTCA-3',

SERPINE1 reverse primer, 5'-TTGAATCCCATAGCTGCTTGAAT-3',

LAP2 forward primer, 5'-CCCCTCGGTCTGACAAAAG-3',

LAP2 reverse primer, 5'-CGCTCTTCGTCCTGAGAA-3',

Lamin B1 forward primer, 5'-GAAAAAGACAACCTCTCGTCGCA-3',

Lamin B1 reverse primer, 5'-GTAAGCACTGATTTCCATGTCCA-3',

P16 forward primer, 5'-ATGGAGCCTTCGGCTGACT-3',

P16 reverse primer, 5'-GTAAGCACTGATTTCCATGTCCA-3',

IL6 forward primer, 5'-ACTCACCTCTTCAGAACGAATTG-3',

IL6 reverse primer, 5'-CCATCTTTGGAAGGTTTCAGGTTG-3'.

RNA-seq library construction and sequencing

Briefly, total RNA was extracted using TRIzol reagent, and genomic DNA was removed using a DNA-free Kit. Library preparation was conducted using a NEBNext® Ultra™ Directional RNA Library Prep Kit for Illumina (New England Biolabs). Quality control and sequencing on Illumina HiSeq X Ten platforms were performed by Novogene Bioinformatics Technology Co., Ltd.

RNA-seq data processing

RNA-seq data processing was performed as previously described (Liu *et al*, 2022b). In brief, low-quality reads and adaptors were first trimmed using TrimGalore (v0.4.4_dev). The remaining clean reads were mapped to the UCSC human hg19 genome using HISAT2 software (v2.2.1). Reads on each annotated gene were counted using featureCounts (v2.0.1). Differentially expressed genes (DEGs) were calculated using DESeq2, if their adjusted *P*-value < 0.05 and

absolute $\text{Log}_2(\text{Fold Change}) > 0.5$. Gene Ontology (GO) term and pathway enrichment analysis were performed using Metascape (<https://metascape.org/>) with P -value less than 0.05. The principal component analysis (PCA) and Euclidian distance were performed using R based on $\text{Log}_2(\text{FPKM}+1)$. The list of aging-related genes was obtained from the Aging Atlas (Aging Atlas, 2021). These DEGs are listed in Datasets EV1–EV3.

4D label-free proteomics

Protein extraction

hMSCs were harvested and lysed with 4 volumes of lysis buffer (8 M urea, 1% protease inhibitor). The cell lysates were centrifuge at 12,000 g for 10 min at 4°C, and protein quantification was measured with a BCA kit.

Trypsin digestion

Equal amounts of protein of each sample was used for enzymatic digestion. Then, 20% trichloroacetic acid (TCA) was added slowly, mixed by vortex, and precipitated at 4°C for 2 h. Protein pellets were obtained by centrifugation at 4500 g for 5 min and wash 2–3 times with precooled acetone. After drying the precipitate, added Triethylammonium bicarbonate (TEAB) to a final concentration of 200 mM. The samples were digested with trypsin at a ratio of 1:50 (protease:protein, m/m) overnight, and then reduced by DTT (5 mM) at 56°C for 30 min. Then, 11 mM iodoacetamide (IAA) was added, and incubated at room temperature for 15 min in the dark to remove excess DTT.

Liquid chromatography-mass spectrometry analysis

The peptides were dissolved in phase A of liquid chromatography mobile phase and separated using NanoElute ultra-high performance liquid phase system. Mobile phase A was supplemented with 0.1% formic acid and 2% acetonitrile; Mobile phase B was supplemented with 0.1% formic acid and 100% acetonitrile. The liquid set was: 0–70 min, 6–24% B; 70–84 min, 24–35% B; 84–87 min, 35–80% B; 87–90 min, 80% B. The flow rate was maintained at 450 nL/min. The peptides were separated by ultra-high performance liquid phase system and injected into Capillary ion source for ionization and then analyzed by timsTOF Pro mass spectrometer. The voltage of ion source was set at 1.75 kV, and the peptide precursor ions and their secondary fragments were detected and analyzed using high-resolution TOF. The scan range of MS was set to 100–1,700. The data acquisition mode was Parallel Accumulation Serial Fragmentation (PASEF) mode. After a first-order mass spectrometer was acquired, PASEF mode was performed for 10 times to collect the second-order spectrum with the charge number of the precursor ion in the range of 0–5, and the dynamic exclusion time of the tandem mass spectrometry scan was set to 30 s to avoid repeated scanning of the precursor ion.

Data analysis

Differentially expressed proteins (DEPs) between $PDI^{-/-}$ vs. $PDI^{+/+}$ were calculated by statistical analysis using unpaired Student's t -test, with the cut-off for P -value < 0.05 and absolute $\text{Log}_2(\text{Fold Change}) > 0.3$. Pathway enrichment analysis was performed using Metascape. The DEPs are listed in Dataset EV4.

Statistical analysis

Data were presented as mean \pm SEM. Statistical analyses were performed using GraphPad Prism software. Comparisons were performed with two-tailed Student's t -test or two-sided Wilcoxon test.

Data availability

The high-throughput sequencing data including RNA-seq and whole-genome sequencing (WGS) generated in this study have been deposited in the Genome Sequence Archive (GSA) in the National Genomics Data Center, Beijing Institute of Genomics (China National Center for Bioinformatics) of the Chinese Academy of Sciences under the accession number HRA002973 (<https://ngdc.cnbc.ac.cn/gsa-human/browse/HRA002973>). The proteomic data have been deposited in the ProteomeXchange Consortium via the PRIDE partner repository with the dataset identifier PXD037244 (<http://proteomecentral.proteomexchange.org/cgi/GetDataset?ID=PX037244>).

Expanded View for this article is available [online](#).

Acknowledgments

We thank Xi'e Wang for administrative assistance, Xi Wang and Ping Liu for helpful discussion, Junying Jia and Shu Meng (Institute of Biophysics, CAS) for their help in the flow cytometry experiments, Lijuan Huang (Institute of Zoology, CAS) for her help in optical *in vivo* imaging. This work was supported by the National Key R&D Program of China (2022YFA1303000, 2021YFA1300800, 2020YFA0804000, 2020YFA0112200); the National Natural Science Foundation of China (32271204, 92254305, 32022033, 81921006, 92149301, 92168201); the Strategic Priority Research Program of CAS (XDB37020303, XDA16010000); the Project for Young Scientists in Basic Research of CAS (YSBR-075, YSBR-076); Tencent Foundation (2021-1045); and the Youth Innovation Promotion Association, CAS, to LW. Cartoons in Figs 2A, 3J, 4A, 4K, 4L, 6H and EV3G were created with BioRender.

Author contributions

Fang Cheng: Formal analysis; investigation; visualization; methodology; writing – original draft. **Qianzhao Ji:** Data curation; formal analysis; visualization. **Lu Wang:** Investigation; methodology. **Chih-chen Wang:** Conceptualization; supervision. **Guang-Hui Liu:** Conceptualization; supervision; funding acquisition; writing – review and editing. **Lei Wang:** Conceptualization; supervision; funding acquisition; writing – original draft; writing – review and editing.

Disclosure and competing interests statement

The authors declare that they have no conflict of interest.

References

- Aging Atlas C (2021) Aging Atlas: a multi-omics database for aging biology. *Nucleic Acids Res* 49: D825–D830
- Appenzeller-Herzog C, Banhegyi G, Bogeski I, Davies KJ, Delaunay-Moisan A, Forman HJ, Grolach A, Kietzmann T, Laurindo F, Margittai E et al (2016) Transit of H_2O_2 across the endoplasmic reticulum membrane is not sluggish. *Free Radic Biol Med* 94: 157–160

- Balch WE, Morimoto RI, Dillin A, Kelly JW (2008) Adapting proteostasis for disease intervention. *Science* 319: 916–919
- Barandalla M, Shi H, Xiao H, Colleoni S, Galli C, Lio P, Trotter M, Lazzari G (2017) Global gene expression profiling and senescence biomarker analysis of hESC exposed to H₂O₂ induced non-cytotoxic oxidative stress. *Stem Cell Res Ther* 8: 160
- Basisty N, Kale A, Jeon OH, Kuehnemann C, Payne T, Rao C, Holtz A, Shah S, Sharma V, Ferrucci L et al (2020) A proteomic atlas of senescence-associated secretomes for aging biomarker development. *PLoS Biol* 18: e3000599
- Bekendam RH, Flaumenhaft R (2016) Inhibition of protein disulfide isomerase in thrombosis. *Basic Clin Pharmacol Toxicol* 119: 42–48
- Bi S, Liu Z, Wu Z, Wang Z, Liu X, Wang S, Ren J, Yao Y, Zhang W, Song M et al (2020) SIRT7 antagonizes human stem cell aging as a heterochromatin stabilizer. *Protein Cell* 11: 483–504
- Bulleid NJ, Ellgaard L (2011) Multiple ways to make disulfides. *Trends Biochem Sci* 36: 485–492
- Burova E, Borodkina A, Shatrova A, Nikolsky N (2013) Sublethal oxidative stress induces the premature senescence of human mesenchymal stem cells derived from endometrium. *Oxid Med Cell Longev* 2013: 474931
- Cai Y, Song W, Li J, Jing Y, Liang C, Zhang L, Zhang X, Zhang W, Liu B, An Y et al (2022) The landscape of aging. *Sci China Life Sci* 65: 2354–2454
- Cheng F, Wang S, Song M, Liu Z, Liu P, Wang L, Wang Y, Zhao Q, Yan K, Chan P et al (2019) DJ-1 is dispensable for human stem cell homeostasis. *Protein Cell* 10: 846–853
- Colton C, Gilbert D (2007) *Reactive oxygen species in biological systems: an interdisciplinary approach*. New York, NY: Springer Science & Business Media
- Curran SP, Ruvkun G (2007) Lifespan regulation by evolutionarily conserved genes essential for viability. *PLoS Genet* 3: e56
- Deng L, Ren R, Liu Z, Song M, Li J, Wu Z, Ren X, Fu L, Li W, Zhang W et al (2019) Stabilizing heterochromatin by DGCR8 alleviates senescence and osteoarthritis. *Nat Commun* 10: 3329
- Diao Z, Ji Q, Wu Z, Zhang W, Cai Y, Wang Z, Hu J, Liu Z, Wang Q, Bi S et al (2021) SIRT3 consolidates heterochromatin and counteracts senescence. *Nucleic Acids Res* 49: 4203–4219
- Fang J, Yang J, Wu X, Zhang G, Li T, Wang X, Zhang H, Wang CC, Liu GH, Wang L (2018) Metformin alleviates human cellular aging by upregulating the endoplasmic reticulum glutathione peroxidase 7. *Aging Cell* 17: e12765
- Fraille M, Eiro N, Costa LA, Martin A, Vizoso FJ (2022) Aging and mesenchymal stem cells: basic concepts, challenges and strategies. *Biology (Basel)* 11: 1678
- Ghosh R, Vinod V, Symons JD, Boudina S (2020) Protein and mitochondria quality control mechanisms and cardiac aging. *Cell* 9: 933
- Han Y, Li X, Zhang Y, Han Y, Chang F, Ding J (2019) Mesenchymal stem cells for regenerative medicine. *Cell* 8: 886
- Harman D (1956) Aging: a theory based on free radical and radiation chemistry. *J Gerontol* 11: 298–300
- Hatahet F, Ruddock LW (2009) Protein disulfide isomerase: a critical evaluation of its function in disulfide bond formation. *Antioxid Redox Signal* 11: 2807–2850
- He Y, Ji Q, Wu Z, Cai Y, Yin J, Zhang Y, Zhang S, Liu X, Zhang W, Liu GH et al (2022) Counteracts human mesenchymal stem cell senescence via maintaining mitochondrial homeostasis. *Protein Cell* 14: 202–216
- Higuchi-Sanabria R, Frankino PA, Paul JW 3rd, Tronnes SU, Dillin A (2018) A futile Battle? Protein quality control and the stress of aging. *Dev Cell* 44: 139–163
- Hipp MS, Kasturi P, Hartl FU (2019) The proteostasis network and its decline in ageing. *Nat Rev Mol Cell Biol* 20: 421–435
- Hisada Y, Garratt KB, Maqsood A, Grover SP, Kawano T, Cooley BC, Erlich J, Moik F, Flick MJ, Pabinger I et al (2021) Plasminogen activator inhibitor 1 and venous thrombosis in pancreatic cancer. *Blood Adv* 5: 487–495
- Hoehne MN, Jacobs L, Lapacz KJ, Calabrese G, Murschall LM, Marker T, Kaul H, Trifunovic A, Morgan B, Fricker M et al (2022) Spatial and temporal control of mitochondrial H₂O₂ release in intact human cells. *EMBO J* 41: e109169
- Hu H, Ji Q, Song M, Ren J, Liu Z, Wang Z, Liu X, Yan K, Hu J, Jing Y et al (2020) ZKSCAN3 counteracts cellular senescence by stabilizing heterochromatin. *Nucleic Acids Res* 48: 6001–6018
- Jang I, Pottekat A, Poothong J, Yong J, Lagunas-Acosta J, Charbono A, Chen Z, Scheuner DL, Liu M, Itkin-Ansari P et al (2019) PDIA1/P4HB is required for efficient proinsulin maturation and ss cell health in response to diet induced obesity. *Elife* 8: e44528
- Jing Y, Zuo Y, Yu Y, Sun L, Yu Z, Ma S, Zhao Q, Sun G, Hu H, Li J et al (2022) Single-nucleus profiling unveils a geroprotective role of the FOXO3 in primate skeletal muscle aging. *Protein Cell* 22: pwac061
- Joung J, Konermann S, Gootenberg JS, Abudayyeh OO, Platt RJ, Brigham MD, Sanjana NE, Zhang F (2017) Genome-scale CRISPR-Cas9 knockout and transcriptional activation screening. *Nat Protoc* 12: 828–863
- Kadokura H, Dazai Y, Fukuda Y, Hirai N, Nakamura O, Inaba K (2020) Observing the nonvectorial yet cotranslational folding of a multidomain protein, LDL receptor, in the ER of mammalian cells. *Proc Natl Acad Sci U S A* 117: 16401–16408
- Khan SS, Shah SJ, Klyachko E, Baldrige AS, Eren M, Place AT, Aviv A, Puterman E, Lloyd-Jones DM, Heiman M et al (2017) A null mutation in SERPINE1 protects against biological aging in humans. *Sci Adv* 3: eaao1617
- Kim K, Hahm E, Li J, Holbrook LM, Sasikumar P, Stanley RG, Ushio-Fukai M, Gibbins JM, Cho J (2013) Platelet protein disulfide isomerase is required for thrombus formation but not for hemostasis in mice. *Blood* 122: 1052–1061
- Kim YM, Youn SW, Sudhakar V, Das A, Chandhri R, Cuervo Grajal H, Kweon J, Leanhart S, He L, Toth PT et al (2018) Redox regulation of mitochondrial fission protein Drp1 by protein disulfide isomerase limits endothelial senescence. *Cell Rep* 23: 3565–3578
- Koivu J, Myllyla R, Helaakoski T, Pihlajaniemi T, Tasanen K, Kivirikko KI (1987) A single polypeptide acts both as the beta subunit of prolyl 4-hydroxylase and as a protein disulfide-isomerase. *J Biol Chem* 262: 6447–6449
- Kong M, Guo L, Xu W, He C, Jia X, Zhao Z, Gu Z (2022) Aging-associated accumulation of mitochondrial DNA mutations in tumor origin. *Life Med* 1: 149–167
- Konno T, Pinho Melo E, Lopes C, Mehmeti I, Lenzen S, Ron D, Avezov E (2015) ERO1-independent production of H₂O₂ within the endoplasmic reticulum fuels Prdx4-mediated oxidative protein folding. *J Cell Biol* 211: 253–259
- Kudryavtseva AV, Krasnov GS, Dmitriev AA, Alekseev BY, Kardymon OL, Sadritdinova AF, Fedorova MS, Pokrovsky AV, Melnikova NV, Kaprin AD et al (2016) Mitochondrial dysfunction and oxidative stress in aging and cancer. *Oncotarget* 7: 44879–44905
- Lei J, Jiang X, Li W, Ren J, Wang D, Ji Z, Wu Z, Cheng F, Cai Y, Yu ZR et al (2022) Exosomes from antler stem cells alleviate mesenchymal stem cell senescence and osteoarthritis. *Protein Cell* 13: 220–226
- Li X, Fang P, Mai J, Choi ET, Wang H, Yang XF (2013) Targeting mitochondrial reactive oxygen species as novel therapy for inflammatory diseases and cancers. *J Hematol Oncol* 6: 19

- Li Y, Wu Q, Wang Y, Li L, Bu H, Bao J (2017) Senescence of mesenchymal stem cells (review). *Int J Mol Med* 39: 775–782
- Liang C, Liu Z, Song M, Li W, Wu Z, Wang Z, Wang Q, Wang S, Yan K, Sun L et al (2021) Stabilization of heterochromatin by CLOCK promotes stem cell rejuvenation and cartilage regeneration. *Cell Res* 31: 187–205
- Liu P, Wang X, Sun Y, Zhao H, Cheng F, Wang J, Yang F, Hu J, Zhang H, Wang CC et al (2022a) SARS-CoV-2 ORF8 reshapes the ER through forming mixed disulfides with ER oxidoreductases. *Redox Biol* 54: 102388
- Liu Z, Ji Q, Ren J, Yan P, Wu Z, Wang S, Sun L, Wang Z, Li J, Sun G et al (2022b) Large-scale chromatin reorganization reactivates placenta-specific genes that drive cellular aging. *Dev Cell* 57: 1347–1368
- Liu X, Liu Z, Wu Z, Ren J, Fan Y, Sun L, Cao G, Niu Y, Zhang B, Ji Q et al (2023) Resurrection of endogenous retroviruses during aging reinforces senescence. *Cell* 186: 287–304
- Lopez-Otin C, Blasco MA, Partridge L, Serrano M, Kroemer G (2023) Hallmarks of aging: an expanding universe. *Cell* 186: 243–278
- Oh J, Lee YD, Wagers AJ (2014) Stem cell aging: mechanisms, regulators and therapeutic opportunities. *Nat Med* 20: 870–880
- Oszejka K, Bieniasz M, Brown G, Swiatkowska M, Bartkowiak J, Szemraj J (2008) Effect of oxidative stress on the expression of t-PA, u-PA, u-PAR, and PAI-1 in endothelial cells. *Biochem Cell Biol* 86: 477–486
- Pak VW, Ezerina D, Lyublinskaya OG, Pedre B, Tyurin-Kuzmin PA, Mishina NM, Thauvin M, Young D, Wahni K, Martinez Gache SA et al (2020) Ultrasensitive genetically encoded indicator for hydrogen peroxide identifies roles for the oxidant in cell migration and mitochondrial function. *Cell Metab* 31: 642–653
- Pan H, Guan D, Liu X, Li J, Wang L, Wu J, Zhou J, Zhang W, Ren R, Zhang W et al (2016) SIRT6 safeguards human mesenchymal stem cells from oxidative stress by coactivating NRF2. *Cell Res* 26: 190–205
- Papadopoulos D, Boulay K, Kazak L, Pollak M, Mallette F, Topisirovic I, Hulea L (2019) mTOR as a central regulator of lifespan and aging. *F1000Res* 8: F1000 Faculty Rev-998
- Parakh S, Atkin JD (2015) Novel roles for protein disulphide isomerase in disease states: a double edged sword? *Front Cell Dev Biol* 3: 30
- Rahman FA, Krause MP (2020) PAI-1, the plasminogen system, and skeletal muscle. *Int J Mol Sci* 21: 7066
- Ramming T, Hansen HG, Nagata K, Ellgaard L, Appenzeller-Herzog C (2014) GPx8 peroxidase prevents leakage of H₂O₂ from the endoplasmic reticulum. *Free Radic Biol Med* 70: 106–116
- Ren X, Hu B, Song M, Ding Z, Dang Y, Liu Z, Zhang W, Ji Q, Ren R, Ding J et al (2019) Maintenance of nucleolar homeostasis by CBX4 alleviates senescence and osteoarthritis. *Cell Rep* 26: 3643–3656
- Ritchie SC, Lambert SA, Arnold M, Teo SM, Lim S, Scepanovic P, Marten J, Zahid S, Chaffin M, Liu Y et al (2021) Integrative analysis of the plasma proteome and polygenic risk of cardiometabolic diseases. *Nat Metab* 3: 1476–1483
- Shan H, Geng L, Jiang X, Song M, Wang J, Liu Z, Zhuo X, Wu Z, Hu J, Ji Z et al (2022) Large-scale chemical screen identifies Gallic acid as a geroprotector for human stem cells. *Protein Cell* 13: 532–539
- Sun G, Zheng Y, Fu X, Zhang W, Ren J, Ma S, Sun S, He X, Wang Q, Ji Z et al (2022a) Single-cell transcriptomic atlas of mouse cochlear aging. *Protein Cell* 14: 180–201
- Sun Y, Li Q, Kirkland JL (2022b) Targeting senescent cells for a healthier longevity: the roadmap for an era of global aging. *Life Med* 1: 103–119
- Swiatkowska M, Szemraj J, Al-Nedawi KN, Pawlowska Z (2002) Reactive oxygen species upregulate expression of PAI-1 in endothelial cells. *Cell Mol Biol Lett* 7: 1065–1071
- Tavernarakis N (2008) Ageing and the regulation of protein synthesis: a balancing act? *Trends Cell Biol* 18: 228–235
- Tu BP, Weissman JS (2004) Oxidative protein folding in eukaryotes: mechanisms and consequences. *J Cell Biol* 164: 341–346
- Ullah I, Subbarao RB, Rho GJ (2015) Human mesenchymal stem cells – current trends and future prospective. *Biosci Rep* 35: e00191
- Vasileiou PVS, Evangelou K, Vlasis K, Fildisis G, Panayiotidis MI, Chronopoulos E, Passias PG, Kouloukoussa M, Gorgoulis VG, Havaki S (2019) Mitochondrial homeostasis and cellular senescence. *Cell* 8: 686
- Wang L, Zhu L, Wang CC (2011) The endoplasmic reticulum sulfhydryl oxidase Ero1beta drives efficient oxidative protein folding with loose regulation. *Biochem J* 434: 113–121
- Wang L, Zhang L, Niu Y, Sitia R, Wang CC (2014) Glutathione peroxidase 7 utilizes hydrogen peroxide generated by Ero1alpha to promote oxidative protein folding. *Antioxid Redox Signal* 20: 545–556
- Wang L, Yu J, Wang CC (2021) Protein disulfide isomerase is regulated in multiple ways: consequences for conformation, activities, and pathophysiological functions. *Bioessays* 43: e2000147
- Wang H, Jiang C, Cai J, Lu Q, Qiu Y, Wang Y, Huang Y, Xiao Y, Wang B, Wei X et al (2022a) Nestin prevents mesenchymal stromal cells from apoptosis in LPS-induced lung injury via inhibition of unfolded protein response sensor IRE1 α . *Life Med* 1: 359–371
- Wang J, Zhou X-F, Wang Y-J (2022b) Continuous antioxidant drug exposure: a bridge from ideal world to real world of therapy for amyotrophic lateral sclerosis. *Life Med* 2: Inac042
- Wang L, Wang X, Lv X, Jin Q, Shang H, Wang CC, Wang L (2022c) The extracellular Ero1alpha/PDI electron transport system regulates platelet function by increasing glutathione reduction potential. *Redox Biol* 50: 102244
- Wang S, Cheng F, Ji Q, Song M, Wu Z, Zhang Y, Ji Z, Feng H, Belmonte JCI, Zhou Q et al (2022d) Hyperthermia differentially affects specific human stem cells and their differentiated derivatives. *Protein Cell* 13: 615–622
- Wang L, Wang C (2023) Oxidative protein folding fidelity and redox status in the endoplasmic reticulum. *Trends in Biochemical Sciences* 48: 40–52
- Westrick RJ, Eitzman DT (2007) Plasminogen activator inhibitor-1 in vascular thrombosis. *Curr Drug Targets* 8: 966–1002
- Wu X, Zhang L, Miao Y, Yang J, Wang X, Wang CC, Feng J, Wang L (2019) Homocysteine causes vascular endothelial dysfunction by disrupting endoplasmic reticulum redox homeostasis. *Redox Biol* 20: 46–59
- Wu Z, Shi Y, Lu M, Song M, Yu Z, Wang J, Wang S, Ren J, Yang YG, Liu GH et al (2020) METTL3 counteracts premature aging via m6A-dependent stabilization of MIS12 mRNA. *Nucleic Acids Res* 48: 11083–11096
- Xu S, Sankar S, Neamati N (2014) Protein disulfide isomerase: a promising target for cancer therapy. *Drug Discov Today* 19: 222–240
- Zhang L, Niu Y, Zhu L, Fang J, Wang X, Wang L, Wang CC (2014) Different interaction modes for protein-disulfide isomerase (PDI) as an efficient regulator and a specific substrate of endoplasmic reticulum oxidoreductin-1alpha (Ero1alpha). *J Biol Chem* 289: 31188–31199
- Zhang W, Li J, Suzuki K, Qu J, Wang P, Zhou J, Liu X, Ren R, Xu X, Ocampo A et al (2015) Aging stem cells. A Werner syndrome stem cell model unveils heterochromatin alterations as a driver of human aging. *Science* 348: 1160–1163
- Zhang J, Zhu Q, Wang X, Yu J, Chen X, Wang J, Wang X, Xiao J, Wang CC, Wang L (2018) Secretory kinase Fam20C tunes endoplasmic reticulum redox state via phosphorylation of Ero1alpha. *EMBO J* 37: e98699

- Zhang X, Liu Z, Liu X, Wang S, Zhang Y, He X, Sun S, Ma S, Shyh-Chang N, Liu F et al (2019a) Telomere-dependent and telomere-independent roles of RAP1 in regulating human stem cell homeostasis. *Protein Cell* 10: 649–667
- Zhang Y, Li T, Zhang L, Shangguan F, Shi G, Wu X, Cui Y, Wang X, Wang X, Liu Y et al (2019b) Targeting the functional interplay between endoplasmic reticulum oxidoreductin-1alpha and protein disulfide isomerase suppresses the progression of cervical cancer. *EBioMedicine* 41: 408–419
- Zhang S, Wu Z, Shi Y, Wang S, Ren J, Yu Z, Huang D, Yan K, He Y, Liu X et al (2022a) FTO stabilizes MIS12 and counteracts senescence. *Protein Cell* 13: 954–960
- Zhang Y, Liu X, Klionsky DJ, Lu B, Zhong Q (2022b) Manipulating autophagic degradation in human diseases: from mechanisms to interventions. *Life Med* 1: 120–148
- Zhao H, Ji Q, Wu Z, Wang S, Ren J, Yan K, Wang Z, Hu J, Chu Q, Hu H et al (2022) Destabilizing heterochromatin by APOE mediates senescence. *Nat Aging* 2: 303–316